

# **Quantifying Land Surface and Subsurface Soil Moisture over Tibetan Plateau**

RUODAN ZHUANG

February 2018

SUPERVISORS:

Dr. Y. Zeng

Prof. Dr. Z. Su





# Quantifying Land Surface and Subsurface Soil Moisture over Tibetan Plateau

RUODAN ZHUANG

Enschede, The Netherlands, February 2018

Thesis submitted to the Faculty of Geo-Information Science and Earth Observation of the University of Twente in partial fulfilment of the requirements for the degree of Master of Science in Geo-Information Science and Earth Observation.

Specialization: Water Resources and Environmental Management

**SUPERVISORS:**

Dr. Y. Zeng

Prof. Dr. Z. Su

**THESIS ASSESSMENT BOARD:**

Dr.ir. S. Salama (Chair)

Prof. M. Menenti (External Examiner)

Ir. A.M. van Lieshout (Course Director WREM)

#### DISCLAIMER

This document describes work undertaken as part of a programme of study at the Faculty of Geo-Information Science and Earth Observation of the University of Twente. All views and opinions expressed therein remain the sole responsibility of the author, and do not necessarily represent those of the Faculty.

## ABSTRACT

The noticeable climate change over Tibetan Plateau and the limited systematic knowledge of land states make it needed to quantify soil moisture accurately. It is hard to study the Plateau scale soil moisture using a single satellite due to its limited lifetime and the misestimation over frozen areas. It is necessary to blend soil moisture products from different sources to extend the data spatial-temporal distribution and reduce the data biases.

The methodology used in this research include surface soil moisture data blending and subsurface soil moisture data prediction. The surface soil moisture data blending method in this research was performed with the constraint of in-situ data climatology based on a least square method. Most of the satellites and blended soil moisture products can produce the top layer soil moisture only, and the relationship between surface and profile soil moisture is non-linear. It is challenging to quantify the profile soil moisture accurately. A depth scaling based on CDF matching was performed to obtain the consistent profile soil moisture from the blended surface soil moisture product.

After output products analysis, it is verified that the methodology used in this research, which includes satellite data merging, in-situ constrained climatology scaling, least squares and triple collocation method based objective merging, is an integrated method for surface and subsurface soil moisture quantifying.

## ACKNOWLEDGEMENTS

Sincerely thanks to my supervisors Dr. Y. Zeng and Prof. Dr. Z. Su. Thank you for your patience, support and guidance. Every meeting or communication was enjoyable.

Sincerely thanks to the thesis assessment board dr.ing. T.H.M. Rientjes, Ir. A.M. van Lieshout, your suggestions and criticisms helped me a lot.

Sincerely thanks to my parents, your love and support give the chance to do the things I love.

Sincerely thanks to H. Zhao, you helped me a lot.

Sincerely thanks to X. Gao, X. Zhao and all the other authors for the precious ideas in all my reference papers.

Thanks to everyone who helped me and gave me support.

Cheers!

# TABLE OF CONTENTS

---

1.	Introduction.....	1
1.1.	Background.....	1
1.2.	Problem Definition .....	2
1.3.	Objective and Research Questions.....	3
1.4.	Innovations.....	3
2.	Material.....	5
2.1.	Study Area.....	5
2.2.	Datasets Description and Pre-processing .....	5
3.	Methodology.....	12
3.1.	Overview .....	12
3.2.	Description of Algorithms.....	13
3.3.	Processing Steps .....	15
4.	Results & Discussion.....	24
4.1.	Satellite Data Merging.....	24
4.2.	Objective Blending.....	27
4.3.	Depth Scaling.....	32
5.	Discussion.....	35
5.1.	Surface Soil Moisture .....	35
5.2.	Subsurface Soil Moisture.....	37
6.	Conclusion & Recommendations .....	40

# LIST OF FIGURES

---

Figure 2.1: The Tibetan Plateau Climatic Zones Classification Map.....	5
Figure 2.2: Start-End Dates Diagram of all the Data Sets for Data Processing .....	5
Figure 2.3: In-situ Network and the Location Scatters Diagrams.....	6
Figure 2.4: AMSRE Soil Moisture Products Retrieval Flowchart .....	7
Figure 2.5: AMSRE soil moisture maps example on 2007-June-05.....	8
Figure 2.6: SMOS soil moisture maps example on 2011-June-05.....	8
Figure 2.7: SMAP soil moisture maps example on 2015-June-05.....	9
Figure 2.8: TP Scale Porosity map.....	10
Figure 2.9: ESACCI Soil Moisture Maps Example on 2007-June-05.....	10
Figure 2.10: ASCAT soil moisture products retrieval flowchart .....	11
Figure 2.11: ERA-Interim Soil Moisture Maps Example on 2007-June-05.....	11
Figure 3.1: Methodology Flowchart .....	12
Figure 3.2: CDF Matching Example Curves .....	13
Figure 3.3: Passive satellites data merging period diagram .....	16
Figure 3.4: Passive products merging flowchart.....	16
Figure 3.5: Error Characterization for Satellites Data Merging over Period S5.....	17
Figure 3.6 Start-End Dates Diagram of all the Data Sets for Objective Blending .....	19
Figure 3.7: Objective Blending Flowchart.....	20
Figure 3.8: Input data for depth scaling.....	22
Figure 3.9: Depth Scaling Methodology Flowchart.....	22
Figure 4.1: Longitude-Time diagram of Original and Scaled SMOS over the entire period .....	25
Figure 4.2: Triplets Number of Scaled AMSR2, SMOS, and SMAP over Merging Period S5.....	25
Figure 4.3: Relative errors of Scaled AMSR2, SMOS, and SMAP over Merging Period S5.....	25
Figure 4.4 Satellites Data Merging example on 05-June-2016 .....	27
Figure 4.5: Example Curves of CDF Matching and Time-longitude Diagrams of SM products .....	28
Figure 4.6: Time series of scaled ERA-Interim, original and scaled PASSIVE products. ....	29
Figure 4.7: Time series of scaled ERA-Interim, original and scaled ACTIVE products.....	29
Figure 4.8: Time-longitude Diagrams of SM Products .....	30
Figure 4.9: Data Number Map .....	30
Figure 4.10 Statistics of triple collocated data .....	31
Figure 4.11: Optimal weights of soil moisture products.....	31
Figure 4.12: Soil Moisture data on 05-June-2007.....	32
Figure 4.13 In-situ Measured surface and subsurface SM Data over Calibration Period.....	34
Figure 4.14: Time-longitude Diagrams of Depth Scaling Reference and Results .....	34
Figure 5.1 Anomalies of Profile Soil Moisture .....	35
Figure 5.2 Taylor Diagram: Inter-comparison between Blended Data and Others .....	36
Figure 5.3 Anomalies of Profile Soil Moisture .....	37
Figure 5.4: Taylor Diagrams: inter-comparison between profile soil moisture data and others. ....	38
Appendix Figure 1: Time Series of In-situ Measured Surface and Subsurface Soil Moisture .....	46
Appendix Figure 2 Anomalies of Blended Surface Soil Moisture.....	48
Appendix Figure 3 Anomalies of Profile Soil Moisture.....	50

## LIST OF TABLES

---

Table 2.1: Characteristics of all the Data Sets for Data Processing.....	6
Table 3.1 Season separation from climatology scaling .....	21
Table 4.1 Prepared Datasets for Satellites Data Merging after Rescaling.....	24
Table 4.2 Averaged Relative Errors of Satellites Data over every Merging Periods.....	26
Table 4.3 Averaged Merging Weights of Satellites Data over every Merging Periods .....	26



# 1. INTRODUCTION

## 1.1. Background

Research on the land surface and subsurface states contribute to research on the freeze-thaw process of Tibetan Plateau. Quantifying land surface and subsurface states is a sufficient way to quantify water and heat balance in the land-atmosphere system and trends of climate change over the Tibetan Plateau. As an essential water source in Asia, Tibetan Plateau has significant effects on the Asian monsoon process, the atmospheric circulation, and the climate patterns (Ma et al., 2017). The noticeable climate changes in past thirty years over Tibetan Plateau (Kang et al., 2010) added demand of rigorous land states quantification. As a crucial land surface and subsurface states variable, soil moisture plays a critical role in the climate system. The variability in soil moisture could be used to reveal feedbacks between the climate system and the hydrological cycle (Su, De Rosnay, Wen, Wang, & Zeng, 2013). Soil moisture physics and dynamics need to be quantified to achieve a deeper understanding of the land-atmosphere interactions (Milly & Dunne, 1994; Polcher, 1995; Reynolds, Jackson, & Rawls, 2000; Drusch, 2007). Rigorous quantification of the energy and water exchanges in the land-atmosphere system can be used for the current numerical weather prediction models validation (Zeng et al., 2016).

Besides, as an important subsurface state, the root-zone profile soil moisture is an important variable in the agricultural system, meteorological system, and hydrological cycle. The saturation of profile soil moisture affects the quantity of water absorbed by crop and plays a significant role in the latent and sensible energy distribution and the precipitation redistribution (Gao et al., 2016). The subsurface soil moisture has a significant spatial variability and has effects on the surface soil moisture through infiltration and capillary phenomenon in a non-linear way (Han, Merwade, & Heathman, 2012).

There are three primary sources for soil moisture data retrieval, which include: in-situ measurements, satellite observations, and model simulations (Zeng et al., 2016). Several in-situ soil moisture observation networks, namely the Third Pole Environment in situ component(TPE) (Ma et al., 2008), the central Tibetan Plateau multi-scale soil moisture and temperature monitoring network (Tibet-Central) (Yang et al., 2013), and the Tibetan Plateau Observatory of soil moisture and soil temperature (Tibet-Obs) (Su et al., 2011), are available over Tibetan Plateau. The currently existing satellite observed soil moisture products include passive and active microwave observations. SMOS: The Soil Moisture and Ocean Salinity (Kerr et al., 2001) and SMAP: the Soil Moisture Active Passive (Entekhabi et al., 2010) are specialised to soil moisture mission. There are also several soil moisture products retrieved from the existing satellites using specific algorithms, for example The Advanced Microwave Scanning Radiometer (AMSR) soil moisture products retrieved by using the Land Parameter Retrieval Model (LPRM) (Owe, de Jeu, & Holmes, 2008), and the Advanced Scatterometer (ASCAT) soil moisture products retrieved by change detection method (Wagner et al., 2013). Besides, the model simulations indicate the reanalysis (land data assimilation) data, which can be provided through the land surface scheme. For example, ERA-Interim: the European Centre for Medium-Range Weather Forecasts interim reanalysis (Dee et al., 2011; Balsamo et al., 2015), and GLDAS: the Global Land Data Assimilation System (Rodell et al., 2004).

The limited lifetime of a single satellite and the period that has complete coverage of the Tibetan Plateau is not sufficient for climate change studies (Wagner et al., 2012). Therefore it is necessary to blend several

available satellite observed data together to obtain a superior soil moisture dataset (Zeng et al., 2016). The blended dataset may solve the problem of misestimation by using specific satellite observed data (e.g. the overestimation of AMSRE and ASCAT over Tibetan Plateau) (Su et al., 2011). For this reason, several merged satellite datasets have been produced by scaling and blending satellite data with model-simulated data, such as ESA-CCI: the Climate Change Initiative soil moisture product (Dorigo et al., 2015) and SMOPS: the Soil Moisture Operational Products System (Zhan, Liu, & Zhao, 2016) from U.S. National Oceanic and Atmospheric Administration (NOAA). These Merged datasets improved the soil moisture data resolution (Owe et al., 2008).

Most of the satellite observed products have not included the profile soil moisture, except for a minority of satellite observed products, such as SMAP Level 4 profile soil moisture product. Usually, the profile data can be obtained from surface soil moisture by using filtering techniques (Petropoulos, 2013). Besides, the CDF matching could be used to operate the depth scaling as well, and it is a robust method to estimate root-zone soil moisture from the surface dataset (Gao et al., 2016).

## 1.2. Problem Definition

The observable climate change in the Tibetan Plateau scale is reshaping the local environment and changing the hydrological cycles (Yang et al., 2014; Kang et al., 2010). The high-quality quantifying of the surface and subsurface states is needed as the Tibetan Plateau is a sensitive area, but the systematic knowledge of the land surface and subsurface states and climate change over it are limited (Ma et al., 2017).

It is hard to study the Tibetan Plateau scale soil moisture content (especially the profile soil moisture) and climate change by using a single satellite-based soil moisture product due to its limited lifetime and the circumscribed performance over frozen and partial-frozen areas (e.g. Tibetan Plateau). To solve this shortcoming, all available data should be used to produce a superior dataset by using appropriate method (e.g. objective blending). Although the existing merged products (e.g. ESA-CCI, SMOPS) improved soil moisture data temporal resolution, the data availability over Tibetan Plateau is limited because of the existing frozen or partial-frozen areas (Owe et al., 2008). Besides, the profile soil moisture has not been included in the results of merged products.

Most of the existing applications of climatology scaling before data blending are performed based on one model simulated soil moisture product without the constraint of in-situ measurement climatology (Liu et al., 2011; Reichle & Koster, 2004; Drusch, Wood, & Gao, 2005; Petropoulos, 2013). It means that the results will be different when the different land surface model would be used, and it may deviate from the real soil moisture dynamics and physics. There was a research on the satellite data blending based on the in-situ climatology scaled reanalysis data and got a high-quality, superior surface soil moisture dataset (Zeng et al., 2016). However, the time range could be extended from 2 years to a longer one by using more available satellite retrieved soil moisture products.

Due to the significant spatial-temporal variability and highly expensive in-situ measurements, it is challenging to quantify the profile soil moisture accurately over Tibetan Plateau. Most of the satellite can produce the top layer soil moisture (<5cm) only, and as well as the existing merged soil moisture products. Moreover, the relationship between surface and profile soil moisture is non-linear, basically (Han, Merwade, et al., 2012).

### **1.3. Objective and Research Questions**

#### **1.3.1. Main objective**

To produce a superior surface soil moisture product by merging satellite observed, reanalysis data and in-situ measured data, and a consistent profile soil moisture product by depth scaling.

#### **1.3.2. Sub-objectives**

- (1) To produce the merged passive and active microwave observation products.
- (2) To obtain the in-situ data climatology by combining in-situ measurement network and the classification of climatic zones over the Tibetan Plateau.
- (3) To constrain the model simulated soil moisture with the in-situ measured data climatology.
- (4) To blend merged passive and active satellite datasets into a consistent dataset with sufficient length, by using the in-situ scaled model simulated datasets.
- (5) To evaluate the quality of blended datasets by anomalies analysis and intercomparison with other products.
- (6) To perform the depth scaling from the surface to root-zone area soil moisture.
- (7) To evaluate the quality of depth scaled profile soil moisture datasets.

#### **1.3.3. Research Questions**

The following research questions ought to be answered to achieve the objectives:

- (1) Do the merged passive and active satellite datasets have a better spatial-temporal coverage over Tibetan Plateau?
- (2) Is there any difference between the results of the scaling with or without the constraint of in-situ data climatology?
- (3) How are the performances of climatology scaling and objective blending methods?
- (4) How is the quality of the blended surface soil moisture dataset?
- (5) How is the performance of the depth scaling method?
- (6) How is the quality of the depth scaled profile soil moisture dataset?

### **1.4. Innovations**

- (1) Merging surface soil moisture products retrieved from satellite observation, model simulation, and in-situ measurement in a relatively extended period (ten years). Previous studies blended only two kinds of datasets (satellite observed, and model simulated) or blended three kinds of datasets in a short period (two years).
- (2) Combining the producing of superior surface soil moisture products and profile soil moisture products to better understand land states over Tibetan in an extended period.



## 2. MATERIAL

### 2.1. Study Area

The average elevation of the Tibetan Plateau exceeding 4000m above sea level, it is an elevated region in the central Asian. The Tibetan Plateau stretches 2500km along longitude and 1000km along latitude. The inferred area is about  $2.5 \times 10^6 \text{ km}^2$  (Yang et al., 2014).

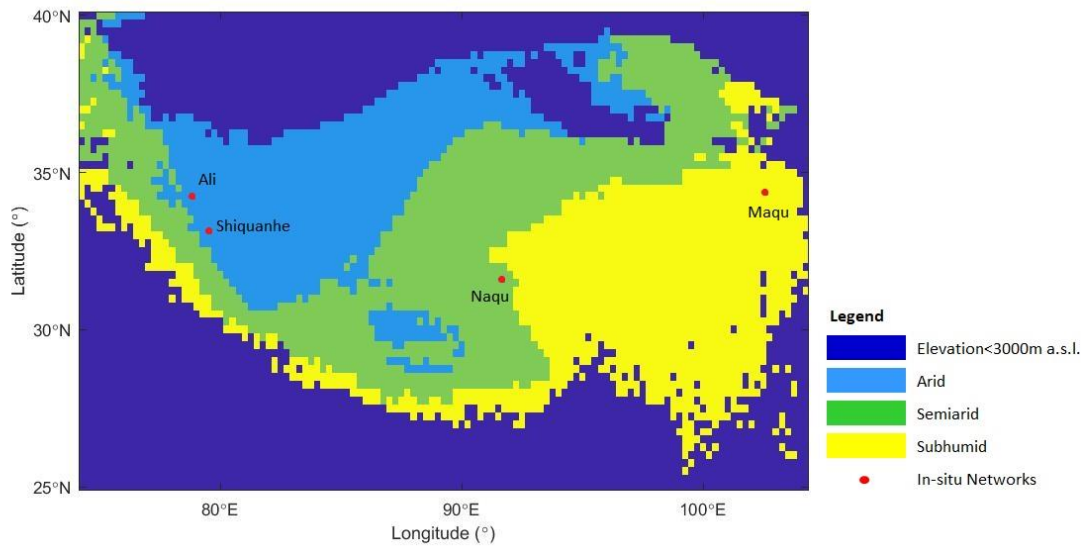


Figure 2.1: The Tibetan Plateau Climatic Zones Classification Map (Source: Zeng et al., (2016))

### 2.2. Datasets Description and Pre-processing

The datasets used in this research and the time range of them are presented in Fig 2.2. There are three different types of soil moisture datasets, include in-situ data (Tibet-Obs), reanalysis data (ERA-Interim), and Satellites datasets (passive: AMSRE, SMOS, AMSR2, and SMAP. Active: ESA-CCI merged active products.). Table 2.1 presents the characteristics of these datasets, including the attributes information of original datasets.

Year	2007	2008	2009	2010	2011	2012	2013	2014	2015	2016	
Month	3 6 9 12	3 6 9 12	3 6 9 12	3 6 9 12	3 6 9 12	3 6 9 12	3 6 9 12	3 6 9 12	3 6 9 12	3 6 9 12	
In-situ	Tibet-Obs			ERA-Interim							
Reanalysis	ERA-Interim										
Passive	AMSRE	SMOS				AMSR2					
	SMOS	AMSR2				SMAP					
	AMSR2	SMAP				ESA-CCI					
	SMAP	ESA-CCI									
Active	ESA-CCI										

Figure 2.2: Start-End Dates Diagram of all the Data Sets for Data Processing

Table 2.1: Characteristics of all the Data Sets for Data Processing

Data sets type	In-situ Data	Reanalysis Data		Satellites Data			
Data sets name	Tibet-Obs	ERA-Interim	AMSRE	SMOS	AMSR2	SMAP	ESA-CCI ACTIVE
Platform	\	\	Aqua	SMOS	GCOM-W1	SMAP	\
Time period used	1-Sep-2010	1-Jun-2007	1-Jun-2007	1-Jun-2010	3-Jul-2012	31-Mar-2015	25-Apr-2013
	31-Aug-2016	31-Dec-2016	3-Oct-2011	31-Dec-2016	31-Dec-2016	31-Dec-2016	31-Dec-2016
Channel used for soil moisture	\	\	6.9 GHz	1.4GHz	6.9 Ghz	1.4GHz	5.2GHz
Original Timporal resolution	15min	Daily	Daily	Daily	Daily	Daily	Daily
Original Spatial resolution (km <sup>2</sup> *km <sup>2</sup> )	\	25*25	25*25	25.8*23	25*25	36*36	25*25
Spatial Coverage	Tibetan	N25-N40, E74-E104	Global	N20-N45, E50-E130	Global	W180-E180, S84-N84	Global
Equatorial crossing time	\	\	Descending	Descending	Descending	Descending	Ascending

### 2.2.1. In-situ

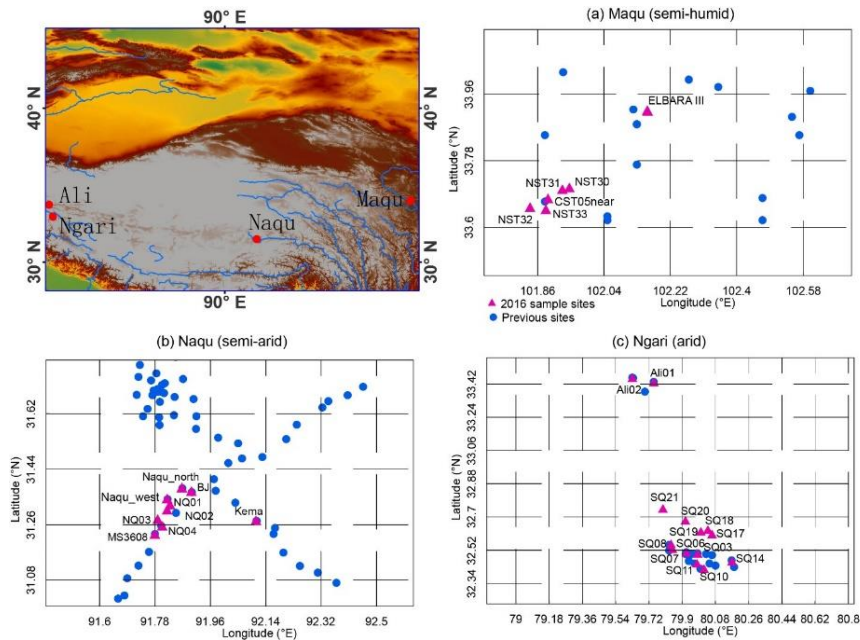


Figure 2.3: In-situ Network and the Location Scatters Diagrams  
(source: Zhao, Zeng, Lv, & Su, (2018))

The Tibetan Plateau Observatory (hereafter as Tibet-Obs) introduced by Su et al. (2011) includes semi-arid Naqu network, subhumid Maqu network and arid Ali-Shiquanhe network. These networks cover three climate zones with 45 observation stations monitoring different depths soil moisture continuously at 15 minutes interval. The surface (5cm) soil moisture data over 2010-Nov-01 to 2011-Oct-31 was used to perform the calibration of surface soil moisture scaling, and it over 1-May-2008 to 2010-Oct-31 was used to validate the blended surface soil moisture data. The surface (5cm) and the profile (average of values at 10cm, 20cm, 40cm, 80cm) soil moisture data over 2014-Sept to 2015-Sept was used to perform the calibration of the depth scaling and it over 2015-Sept, and 2016-Sept was used to validating the final profile soil moisture product. The averaged soil moisture data series from various observation networks were used to produce in-situ measured input data of each network.

2.2.2. Satellite Data

2.2.2.1. AMSR-E

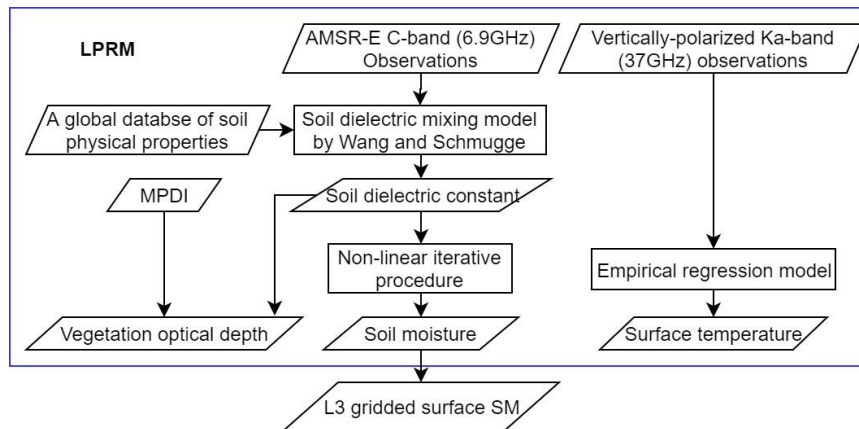


Figure 2.4: AMSRE Soil Moisture Products Retrieval Flowchart  
 (Source: Njoku, Jackson, Lakshmi, Chan, & Nghiem, (2003) )

The VUA-NASA retrieval soil moisture product (hereafter AMSR-E) used in this research were derived from the Advanced Microwave Scanning Radiometer-Earth Observing System (Owe et al., 2008; Njoku, Jackson, Lakshmi, Chan, & Nghiem, 2003). The passive microwave observed brightness temperature (e.g. AMSR-E resampled brightness temperature product AE\_L2A) were processed by using LPRM: The Land Parameter Retrieval Model. There are three land surface parameters related to the LPRM, which include: land surface temperature, vegetation water content, and soil dielectric constant. The land surface temperature was obtained from the Ka-band (36.5 GHz) (Holmes, de Jeu, Owe, & Dolman, 2009). The vegetation optical depth was derived from the soil dielectric constant (Meesters, De Jeu, & Owe, 2005). The soil dielectric constant was derived from the soil dielectric mixing model with a global database of soil physical properties (Wang & Schmugge, 1980). Then the soil moisture was derived from a forward radiative transfer model using a nonlinear iterative optimisation method and the microwave polarisation difference index of the brightness temperature (Mo, Choudhury, Schmugge, Wang, & Jackson, 1982). The two products provided by LPRM include volumetric soil moisture retrieved from C-band and X-band observations. C-band over Tibetan has less signal attenuation from atmosphere and vegetation and less radio-frequency interference ( Njoku, Ashcroft, Chan, & Li, 2005 ). So, the soil moisture products used in this research were derived from C-band with a time range of 01-July-2007 to 03-Oct-2011 and provided on a 25km×25km grid. The original spatial coverage starts from W 180° to E 180°, from N 90° to S 90°, they were 720 rows×1440 columns before subsetting. After subsetting, the grids became 61 rows×121 columns (E 74°- E 104°, N 25°- N 40°). Only the descending mode (night time: 01:30 am local time) AMSR-E products were used because there are fewer uncertainties caused by temperature variations during night-time (Dente, Ferrazzoli, Su, van der Velde, & Guerriero, 2014).

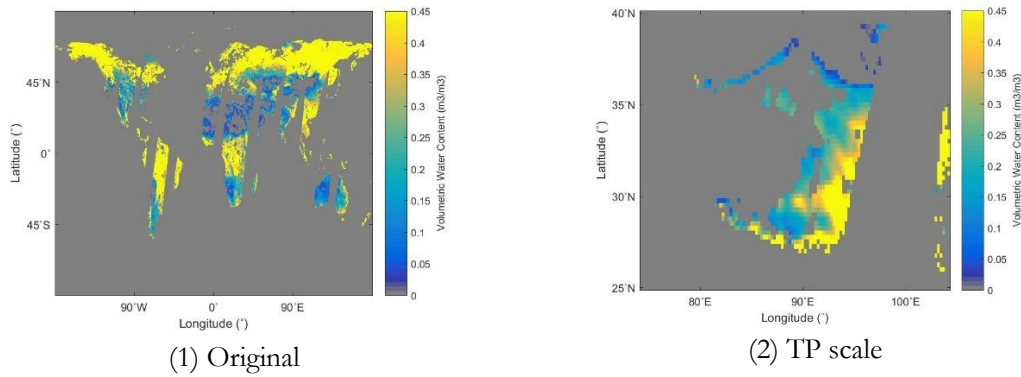


Figure 2.5: AMSRE soil moisture maps example on 2007-June-05

### 2.2.2.2. AMSR-2

The AMSR-2 datasets are derived from the Advanced Microwave Scanning Radiometer 2 loaded on the Water GCOM-W1 satellite launched by JAXA: the Japan Aerospace Exploration Agency (Keiji Imaoka et al., 2010). The AMSR-2 is a follow-up of AMSR-E, and it has worked together with AMSR-E since 3 July 2012 to provide a long-term satellite observation (Imaoka et al., 2012). LPRM was used to retrieve soil moisture products as well, the steps are similar with AMSR-E, but the input datasets are from the AMSR-2 brightness temperatures with a matched spatial-resolution. The descending daily products used in this study were the night-time products over the period of 03-July-2012 to 31-Dec-2016. The original spatial coverage, the spatial resolution, and the subsetting approach are same with AMSR-E.

### 2.2.2.3. SMOS

The SMOS soil moisture data were derived from the European Soil Moisture and Ocean Salinity satellite by France National Centre for Space Studies (cnes). As one of the Earth Explorer Opportunity Missions from ESA: the European Space Agency, the SMOS satellite was launched successfully with a 1.4 GHz L-Band radiometer as the baseline payload on 2-Nov-2009 (Kerr et al., 2010). One of the scientific objectives is retrieving the global soil moisture over land surfaces with better accuracy (4% volumetric soil moisture) in a spatial resolution less than 50 km. The SMOS operates with a revisit time less than three days and provides global coverage with an ascending orbit (6:00 am) and a descending orbit (6:00 pm) (Kerr et al., 2012). The L-band microwave emission is obtained from a zero-order radiative transfer equation, and the L-MEB biosphere model is the retrieval algorithm of SMOS (Wigneron et al., 2007). The multiangular observation helped SMOS obtain the soil moisture and ancillary information simultaneously (Wigneron et al., 2007; Zeng et al., 2015). As a re-sampled and temporally accumulated data, the Level 3 one-day descending surface soil moisture products located over 01-June-2010 to 31-Dec-2016 were used in this research.

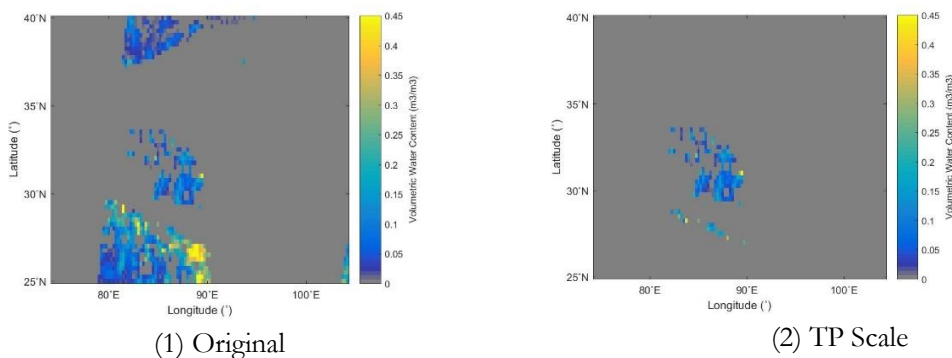


Figure 2.6: SMOS soil moisture maps example on 2011-June-05

The original spatial coverage of the downloaded data starts from E 50° to E 130°, from N 20° to N 45°, they were 108 rows×310 columns before subsetting. Moreover, the original data were multiplied by the scale factor 0.000030519 to obtain the real soil moisture values. After subsetting them to E 74° - E 104°, N 25° - N 40°, and resampling to 25\*25km resolution, the grids became 61 rows ×121 columns. All the satellites data and reanalysis data in this research were resampled to 25\*25km resolution in both latitude and longitude extension. This is a trade-off between the higher resolution scatter meter data and the generally coarser passive microwave observations. The resolution of the products is often adopted by land surface models. The linear interpolation was used in resampling step as it is the most widely used interpolation algorithm for reconstruction since it produces reasonably good results at moderate cost.

#### 2.2.2.4. SMAP

The SMAP soil moisture data was retrieved from L-band (1.41 GHz) of the passive microwave radiometer of Soil Moisture Active Passive mission. NASA (National Aeronautics and Space Administration) launched the SMAP satellite on 31-Jan-2015. The soil moisture data was derived from L-band brightness temperature. The SMAP soil moisture observation target is a volumetric accuracy of  $0.04\text{m}^3\cdot\text{m}^{-3}$  in the top layer of land surface every two to three days (Akbar & Moghaddam, 2015; Panciera et al., 2014). The tau-omega model is the retrieval algorithm of soil moisture retrieval, and it used at a constant incident angle. The open water area has been corrected, then the retrieval algorithm was operated (O'Neill, Chan, Njoku, Jackson, & Bindlish, 2014).

The SMAP product used in this research is a SMAP L3 Radiometer Global Daily data of descending orbit (6:00 pm to 6:00 am) SMAP radiometer-based soil moisture retrieval on the global 36-km Equal-Area Scalable Earth (EASE 2.0) Grid designed by the National Snow and Ice Data Center (NSIDC). The data used here is from 31-March-2015 to 31-Dec-2016 over Tibetan Plateau. The original spatial coverage of the downloaded data starts from W 180° to E 180°, from N 84° to N 84°, they were 406 rows×964 columns before subsetting. After subsetting them to E 74° - E 104°, N 25° - N 40°, and resampling to 25\*25km resolution, the grids became 61 rows ×121 columns. The linear interpolation was used in resampling step as well.

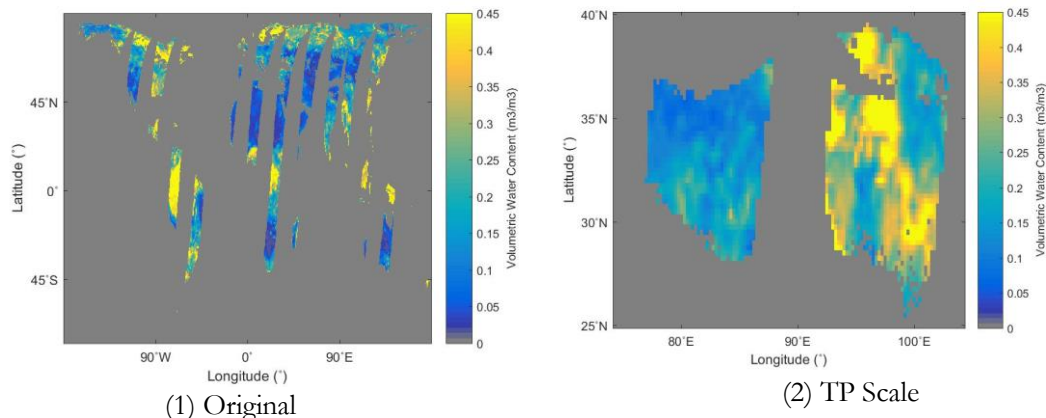


Figure 2.7: SMAP soil moisture maps example on 2015-June-05

#### 2.2.2.5. ESA-CCI Merged ACTIVE Products

The ESA-CCI (ESA Climate Change Initiative) merged ACTIVE products are merged by Metop-A and Metop-B ASCAT products. The ACTIVE soil moisture products used in this research were obtained from 01-June-2007 to 31-Dec-2016. The original products are provided as saturation degrees (0% - 100%), and it should be converted to the volumetric soil moisture. The porosity values over Tibetan Plateau were used

to multiply saturation degrees yields the volumetric soil moisture with a unit of  $\text{m}^3\cdot\text{m}^{-3}$ . The porosity values were provided by ESA-CCI.

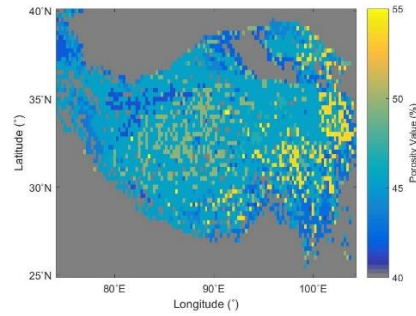


Figure 2.8: TP Scale Porosity map

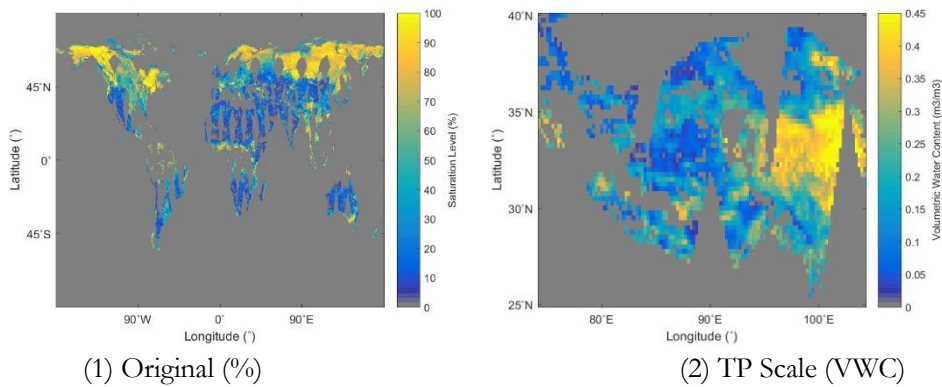


Figure 2.9: ESACCI Soil Moisture Maps Example on 2007-June-05

As a real aperture backscatter radar, the Advanced Scatterometer (ASCAT) is being loaded on the Meteorological Operational (METOP) satellites (Wagner et al., 2013). There are three METOP satellites operate as a polar-orbiting satellites series. METOP-A and METOP-B were launched in Oct-2006 and Sept-2012. They are operating in parallel in a dual constellation, and it could provide a better spatial and temporal resolution. METOP-C will be launched in 2018, and it will work together with METOP-A and METOP-B to deliver a full-coverage ASCAT backscatter observation (Zeng et al., 2015). The ASCAT observes the land surface in both ascending (9:30 pm) and descending (9:30 am) mode by operating in 5.255 GHz C-band at VV polarisation (Wagner et al., 2013).

A change detection method based on time series was used to retrieve soil moisture from ASCAT backscatter observations (Bartalis, Naeimi, & Wagner, 2008). The retrieve algorithm was developed by Wagner et al. (2013) and Naeimi, Scipal, Bartalis, Hasenauer, & Wagner (2009). Although the effect of vegetation on the active microwave observation is still poorly understood, the C-band has been found has a significant response of soil even in the vegetated areas when the incidence angle is low (Su, Troch, & DeTroch, 1997; Wen & Su, 2003). The different responses of three scatterometer antenna geometries to the vegetation was used to model sensitivity of the backscattering signal to the seasonal vegetation effect. The backscattering was normalized by using a reference incidence angle. The dry land surface condition is the highest backscattering value over the entire research period, while the lowest backscattering value refers to the saturated soil condition.

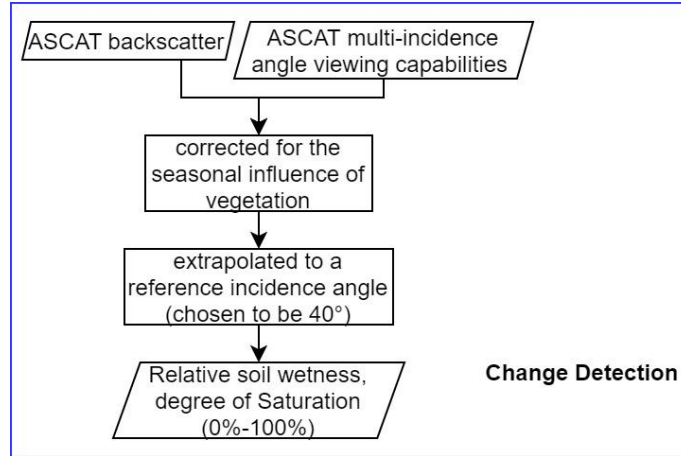


Figure 2.10: ASCAT soil moisture products retrieval flowchart

**2.2.3. Reanalysis Product**

**2.2.3.1. ERA-Interim**

ERA-Interim soil moisture product (hereafter as ERA-Interim) is a part of Land Data Assimilation System produced by ECMWF: the European Centre for Medium-Range Weather Forecasts (Dee et al., 2011). The soil moisture simulated volumetric soil moisture content in four layers separately, and the daily average soil moisture of the first layer (0-7 cm) is the one to be used in the proposed research. As the reference dataset, the reanalysis data requires a comparable spatial (25km) and temporal (daily) resolution with satellites data to be used in climatology scaling (Liu et al., 2011). So, the daily ERA-Interim soil moisture product to be used here has been interpolated to a comparable resolution of 25km instead of the original coarse resolution (80km) while retrieving it from ECMWF web page.

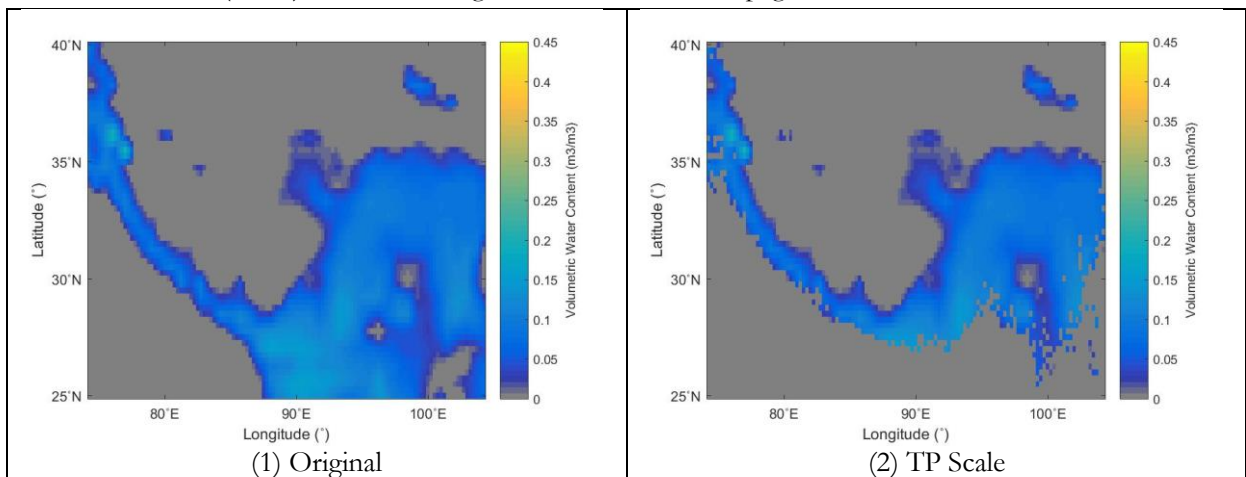


Figure 2.11: ERA-Interim Soil Moisture Maps Example on 2007-June-05

### 3. METHODOLOGY

#### 3.1. Overview

The processing steps in this research include *Satellites Data Merging*, *Objective Blending*, and *Depth Scaling*. The figure 3.1 Methodology flowchart presents an overview of processing steps. In the flowchart, the TP indicates the Tibetan Plateau; The SSM and PSM indicate surface and profile soil moisture. The calibration period of surface soil moisture data blending is from 01-Sept-2014 to 31-Aug-2015 (one year include four full seasons), the calibration period of sub-surface soil moisture data is from 01-Sept-2013 to 31-Aug-2015 and the surface soil moisture blending period is from 01-Jan-2007 to 31-Dec-2016 (ten years) as well as the depth scaling period.

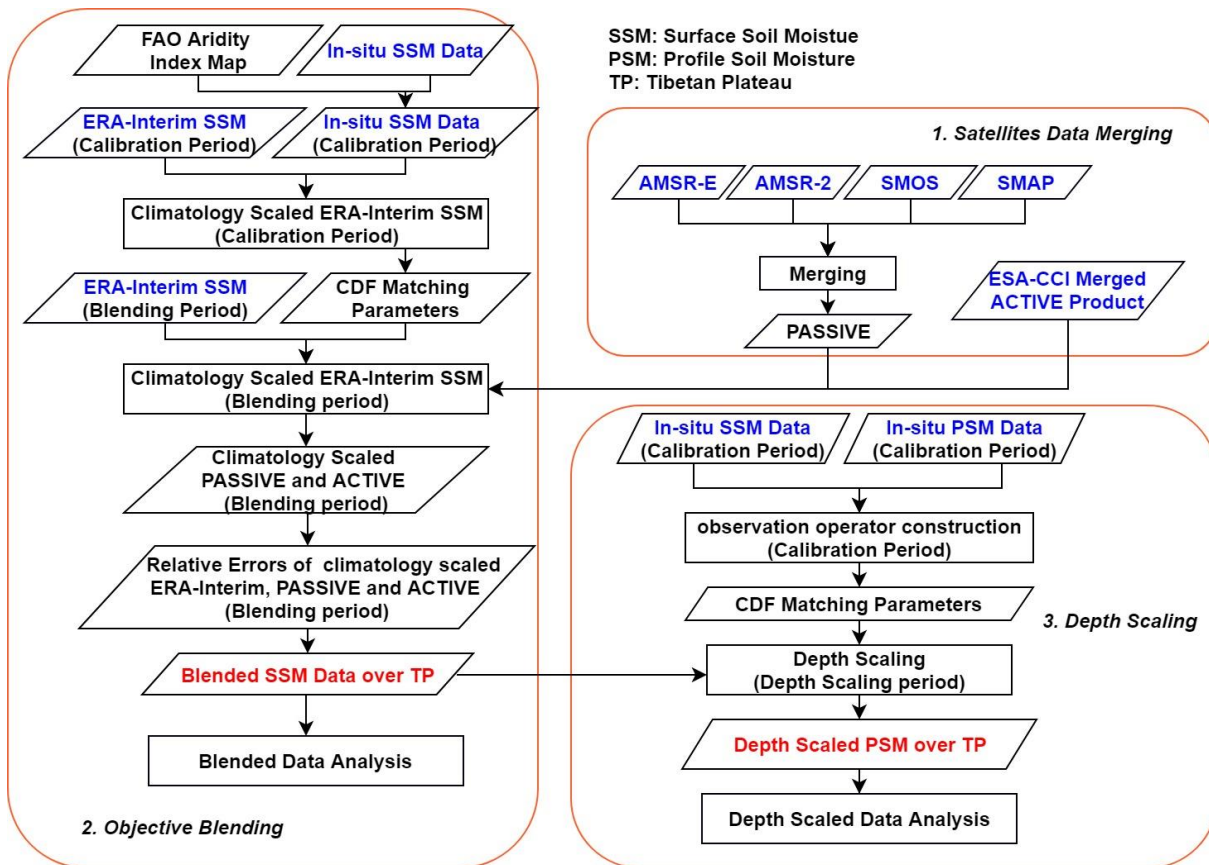


Figure 3.1: Methodology Flowchart

As presented in the methodology flowchart and explained in the section “2.2 Datasets Description”, the input datasets (indicated as blue text) include in-situ measured soil moisture data, reanalysis soil moisture data ERA-Interim and satellites observed data. After *Satellite Data Merging*, the original single satellites data were merged into PASSIVE and ACTIVE two different products. To perform the *Objective Blending*, a Climatology scaling was executed in advance to scale the PASSIVE and ACTIVE products by the in-situ scaled reanalysis data. Then the scaled satellites data and scaled reanalysis data were blended into a consistent surface soil moisture product. Then, a *Depth Scaling* was performed to produce the profile soil moisture products. In the end, an analysis of the final surface and profile soil moisture products was performed as a validation step. The following sections are the description of algorithms and detailed explanations of the processing steps.

### 3.2. Description of Algorithms

Three main statistical approaches were used in this research, include CDF matching, least squares method and triple collocation method. The core process of *Satellites Data Merging* and *Objective Blending* could be performed using the least squares method, which is explained in section 3.2.2. The way to ensure the input observations condition of the least squares method is CDF matching, which is explained in section 3.2.1. Moreover, it also used to perform the *Depth Scaling*. The way to determine the error variances required in the least squares method is triple collocation, which is explained in section 3.2.3.

#### 3.2.1. CDF Matching

Cumulative distribution function matching (CDF matching) was used in all the three main steps to correct the systematic difference among data sets which is necessary for the following weighted merging step. For *Satellites Data Merging*, the passive satellite's data (i.e. SMOS, AMSR2, and SMAP) were scaled using CDF matching based on the reference product AMSRE. For *Objective Blending*, the ERA-Interim data were scaled by in-situ data climatology first; then the PASSIVE and ACTIVE products were scaled by the scaled ERA-Interim. In *Depth Scaling*, CDF matching was used to generate the observation operator to obtain profile soil moisture data from surface soil moisture data.

The CDF matching approach has been widely used for removing systematic differences between two series, such as bias reduction in satellite-observed surface soil moisture (Liu et al., 2011; Drusch, Wood, & Gao, 2005; Reichle & Koster, 2004; Petropoulos, 2013). For example, the satellite observed time series can be rescaled through this approach, so that its CDF matches the CDF of the in-situ measured data. The method can also be used to transfer the different areas data (Gao et al., 2013) and upscale the point data measurements (Han, Heathman, Merwade, & Cosh, 2012). Besides, Gao et al. (2016) did the depth scaling by the construction of observation operators using CDF matching.

To operate CDF matching, five main steps should be operated. The first step is ranking the reference data, and the to-be scaled data. Second, calculate the differences between the corresponding data of two datasets. Third, plot the calculated differences against the to-be scaled series. Next, the piece-wise linear CDF matching technique can be used in the satellite observed data merging and the climatology scaling (Zeng et al., 2016). It is a technique to perform linear regression analysis segment by segment for a certain number of segments on the CDF curve. The last step is using the linear parameters to scale the to-be scaled data for each segment (Brocca et al., 2011). Following Figure is example CDF curves of reference data (ref), original observation (obs), and scaled observation (Scaled obs). The CDF curve of original observation is different with the reference, while the CDF curve of scaled observation shows a similar pattern with the CDF curve of reference data after scaling. The systematic difference between the original observation and the reference data has been eliminated.

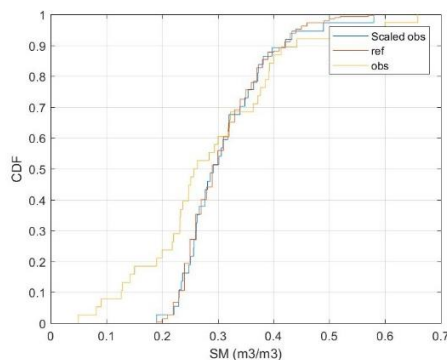


Figure 3.2: CDF Matching Example Curves

Also, among four common scaling methods (linear regression, linear rescaling, MIN/MAX correction, and CDF matching), the CDF matching showed a better performance in some cases (Petropoulos, 2013). Moreover, it requires at least one year to calibrate this statistical approach due to the high number of parameters used in the operators (Liu et al., 2011). One-year in-situ measured data is available to do the calibration in this approach.

### 3.2.2. Least Squares Merging

Least squares method was employed in this study to perform *Satellites Data Merging* and *Objective Blending*. The objective is determining merged soil moisture values from two or three independent datasets. In *Satellites Data Merging* step, it executed over several time periods to merge different satellites observations into one consistent product. In *Objective Blending*, it used to blend the scaled satellite's data and the scaled ERA-Interim data.

The least squares method is one of the most widely used data assimilation methods (Talagrand, 1997). Since it was shaped into the current form by Kalman, (1960), it has been used in numerous studies (Sorenson, 1970). It was used to blend remote sensed and model simulated soil moisture products by Yilmaz, Crow, Anderson, & Hain, (2012).

To determine the merged soil moisture product  $SM_m$  from three independent soil moisture products ( $SM_a, SM_b, SM_c$ ) of the form

$$SM_a = \alpha SM + e_a \quad 3-1 \text{ a}$$

$$SM_b = \alpha SM + e_b \quad 3-1 \text{ b}$$

$$SM_c = \alpha SM + e_c \quad 3-1 \text{ c}$$

where  $e_a, e_b, e_c$  are zero-mean observational errors, and  $SM$  is the assumed true value of soil moisture. When the statistical means of  $e_a, e_b, e_c$  are 0, the variance of them are known and expressed as  $\sigma_a^2, \sigma_b^2, \sigma_c^2$ . As the datasets errors are assumed independent, the error covariances can be ignored. And also the solution of least squares can be simplified. In this research, all the datasets used to perform least squares method are independent as they are obtained from different instruments. The coefficient  $\alpha$  indicates that the slopes of linear relationships between each soil moisture products and true values should be the same, which means the datasets have no systematic biases. It is required for obtaining the least squares solution and has been satisfied by performing the CDF matching before datasets merging (in this research  $\alpha = 1$ ).

When the target product is merged as a linear combination of single products, the equation of data merging can be expressed as:

$$SM_m = \omega_a SM_a + \omega_b SM_b + \omega_c SM_c \quad 3-2$$

where  $\omega_a, \omega_b, \omega_c$  are the relative weights of data sets a, b, c, and  $SM_m$  is the target merged product.

When  $\omega_a + \omega_b + \omega_c = 1$ , the merged product is unbiased. It is a constraint of the solution to the estimation error variance minimization problem. So, the solution to minimize the error variance of  $SM_m$  relate to weights  $\omega_a, \omega_b, \omega_c$ , and the weights could be calculated from relative error variance  $\sigma_a^2, \sigma_b^2, \sigma_c^2$ . The to be minimised error variance of  $SM_m$  can be expressed as

$$\sigma^2 = \omega_a^2 \sigma_a^2 + \omega_b^2 \sigma_b^2 + \omega_c^2 \sigma_c^2 \quad 3-3$$

Assume  $\partial \sigma^2 / \partial \omega_a^2 = 0$  and  $\partial \sigma^2 / \partial \omega_c^2 = 0$ , the equations to determine the relative weights by using relative errors are presented below:

$$\omega_a = \frac{\sigma_b^2 \sigma_c^2}{\sigma_a^2 \sigma_b^2 + \sigma_a^2 \sigma_c^2 + \sigma_b^2 \sigma_c^2} \quad 3-3 \text{ a}$$

$$\omega_b = \frac{\sigma_a^2 \sigma_c^2}{\sigma_a^2 \sigma_b^2 + \sigma_a^2 \sigma_c^2 + \sigma_b^2 \sigma_c^2} \quad 3-3 \text{ b}$$

$$\omega_c = \frac{\sigma_a^2 \sigma_b^2}{\sigma_a^2 \sigma_b^2 + \sigma_a^2 \sigma_c^2 + \sigma_b^2 \sigma_c^2} \quad 3-3 \text{ c}$$

The method can also work in two datasets situation, the equations are presented below:

$$\omega_a = \frac{\sigma_b^2}{\sigma_a^2 + \sigma_b^2} \quad 3-4 \text{ a}$$

$$\omega_b = \frac{\sigma_a^2}{\sigma_a^2 + \sigma_b^2} \quad 3-4 \text{ b}$$

### 3.2.3. Triple Collocation Analysis

Triple collocation was used in both *Satellites Data Merging* and *Objective Blending* to determine the relative errors (i.e. error variances) of each input observations. In *Satellite Data Merging* step, the triple collocation method was used to calculate the relative errors of every single satellites data by using ERA-Interim data and ESA-CCI ACTIVE products over every single merging period. In *Objective Blending*, triple collocation method was used to generate the relative errors of the scaled ERA-Interim, scaled PASSIVE and scaled ACTIVE products. The relative errors were used to determine the relative weights of each product for subsequent satellites data merging or soil moisture products blending steps using least squares method. Triple collocation is an error estimation method which can be used to estimate random error variances and systematic biases in different datasets without reliable reference data sets. It improved the accuracy of calibration or validation when compared with the dual comparisons which were widely used before. To operate the triple collocation method, three independent datasets should be used jointly to constrain the relative errors determining (Stoffelen, 1998). The triplets to perform triple collocation analysis are three collocated and independent data sets. The error variance can be presented as:

$$\sigma_{\varepsilon_a}^2 = \sigma_a^2 - \frac{\sigma_{a,b} \sigma_{a,c}}{\sigma_{b,c}} \quad 3-5 \text{ a}$$

$$\sigma_{\varepsilon_b}^2 = \sigma_b^2 - \frac{\sigma_{b,a} \sigma_{b,c}}{\sigma_{a,c}} \quad 3-5 \text{ b}$$

$$\sigma_{\varepsilon_c}^2 = \sigma_c^2 - \frac{\sigma_{a,c} \sigma_{b,c}}{\sigma_{a,b}} \quad 3-5 \text{ c}$$

where  $\sigma_a^2, \sigma_b^2, \sigma_c^2$  are the data variances, and  $\sigma_{\varepsilon_a}^2, \sigma_{\varepsilon_b}^2, \sigma_{\varepsilon_c}^2$  are the errors variances.  $\sigma_{a,b}, \sigma_{b,c}, \sigma_{a,c}$  are data covariance.

## 3.3. Processing Steps

### 3.3.1. Satellite Data Merging

*Satellites Data Merging* aims to merge all the available passive observations data into one PASSIVE product, and all the active observations data into one ACTIVE product. As explained in section “2.2 Datasets Description and Pre-processing”, the available passive satellites data include AMSRE, SMOS, AMSR2, and SMAP. As for active satellites observations, I was planned to merge Metop-A and Metop-B ASCAT products into the ACTIVE products, but when I tried to download and process the ASCAT products,

some problems occurred. Moreover, ESA-CCI merged ACTIVE products were obtained in the same way as I planned. So, the ESA-CCI Merged ACTIVE products were used as the input of the second step *Objective Blending* directly. In this section, the detailed merging steps of passive satellites data are explained.

The passive satellites datasets include AMSRE, SMOS, AMSR2, and SMAP as explained, and the available time of them are different. These datasets were merged where more than one dataset exist, then they were concatenated in sequence. The merging period of passive satellites data has been decided based on the available period of every single satellite (Figure 3.3). The first merging period (S1) includes only AMSRE data, and the third merging period (S3) has only SMOS data, which can be used directly as a part of the PASSIVE product. The second part of the PASSIVE product (merging period S2) was merged by AMSRE and SMOS. The fourth part (S4) was merged by SMOS and AMSR2. Moreover, The fifth part (merging period S5) was merged by SMOS, AMSR2 and SMAP. The steps of merging passive microwave datasets (AMSRE, SMOS, AMSR2, SMAP) are presented in Figure 3.4. The main sub-steps include Rescaling using CDF Matching, error characterisation using Triple Collocation Analysis and merging using the least squares method, and they are explained step by step in the following sections.

Year	2007			2008			2009			2010			2011			2012			2013			2014			2015			2016				
Month	3	6	9	12	3	6	9	12	3	6	9	12	3	6	9	12	3	6	9	12	3	6	9	12	3	6	9	12	3	6	9	12
AMSRE	[Blue]									[Blue]			[Blue]			[Blue]			[Blue]			[Blue]			[Blue]			[Blue]				
SMOS	[White]									[Blue]			[Blue]			[Blue]			[Blue]			[Blue]			[Blue]			[Blue]				
AMSR2	[White]									[White]			[White]			[Blue]			[Blue]			[Blue]			[Blue]			[Blue]				
SMAP	[White]									[White]			[White]			[White]			[White]			[Blue]			[Blue]			[Blue]				
	S1						S2			S3			S4						S5													

Figure 3.3: Passive satellites data merging period diagram

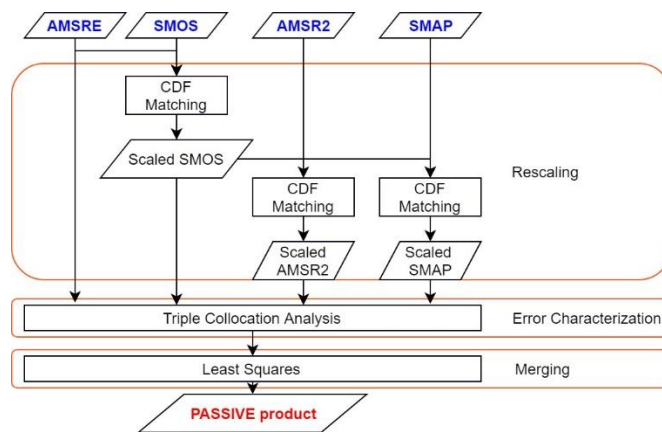


Figure 3.4: Passive products merging flowchart

**(1) Rescaling**

Differences in sensors specifications, particularly in microwave frequency and spatial resolution, result in different absolute soil moisture values from AMSR2, SMOS, SMAP, AMSR-E. Even though AMSR2 and AMSR-E have a similar frequency (i.e., C-band), their absolute values are different. I scaled the datasets into a common data climatology before I performed the satellites data merging. Rescaling of all the passive microwave soil moisture observations to the climatology of AMSR-E. Rescaling was performed using cumulative distribution function (CDF) matching, which was explained in section 3.2.1.

Based on previous research by Liu et al., (2012), the AMSR-E soil moisture retrievals were identified as more accurate than the other passive products due to the relatively low microwave frequency and high temporal and spatial resolution of the sensor. Thus, soil moisture retrievals from AMSR-E are selected as the reference to which soil moisture retrievals from SMOS, AMSR2, and SMAP are scaled. In Figure 3.3, the box with red border indicates the overlap period of the AMSRE (scaling reference) and SMOS, and SMOS (dark blue bar) overlaps with all the other satellites. So, as indicated in the flowchart Figure 3.4, the scaled SMOS is the reference to all the others.

## (2) Error Characterization

Error characterisation aims to obtain the relative errors of all the to be merged datasets using triple collocation analysis. A necessary condition for the feasibility of triple collocation method is statistically significant, which requires determination of the minimum correlation coefficient values range. Usually, the p-values corresponding to statistical significant is  $<0.05$ . Others, it has been discussed by Zwieback, Scipal, Dorigo, & Wagner, (2012) that 100 triplets numbers are the minimum sample size for a reliable triple collocation method calculation. Under these two conditions, the corresponding minimum correlation coefficient should be  $>0.15$ . The primary procedures are illustrated in the flowchart in Figure 3.5. First, as indicated in Figure 3.5, the three-located data number over each merging period were checked. Then, the minimum correlation coefficients of SMOS, AMSR2, and SMAP against ACTIVE and ERA-Interim were calculated to check the significant level. Then the error variance of each pixel where statistical significant were calculated using triple collocation method. After triple collocation analysis, the relative errors of each dataset were used to perform the least squares method.

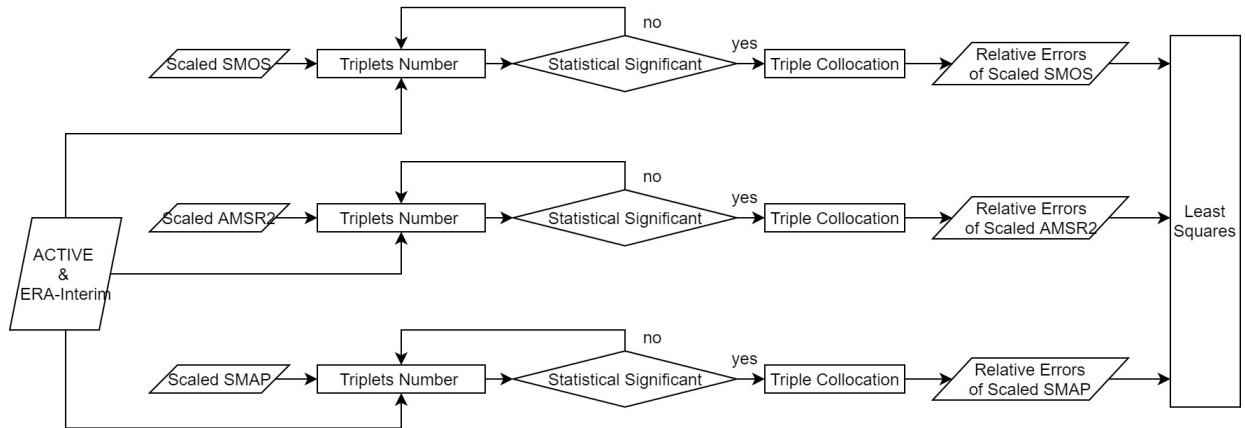


Figure 3.5: Error Characterization for Satellites Data Merging over Period S5 (31-Mar-2015 to 31-Dec-2016)

Error characterization was performed over every single merging period after rescaling. Satellites Data over S5 are served as an example in the following explanation, the error variance of three individual passive products (scaled SMOS, AMSR2 and SMAP) was characterized using triple collocation analysis. Triple collocation analysis was explained detailed in section 3.2.3. This method requires the errors of the three data sets to be uncorrelated. Therefore triplets always comprise of an active data set, a passive data set, and a model simulated dataset, which is commonly assumed to fulfil this requirement (Dorigo et al., 2010). So, the ESA-CCI Merged ACTIVE product and ERA-interim product over the same period were used to complement the triplets. The equations for determining the error variances are presented below:

$$\sigma_{\varepsilon_{SMOS}}^2 = \sigma_{SMOS}^2 - \frac{\sigma_{SMOS,ACTIVE}\sigma_{SMOS,ERA}}{\sigma_{ACTIVE,ERA}} \quad 3-6 a$$

$$\sigma_{\varepsilon_{AMSR2}}^2 = \sigma_{AMSR2}^2 - \frac{\sigma_{AMSR2,ACTIVE}\sigma_{AMSR2,ERA}}{\sigma_{ACTIVE,ERA}} \quad 3-6 \text{ b}$$

$$\sigma_{\varepsilon_{SMAP}}^2 = \sigma_{SMAP}^2 - \frac{\sigma_{SMAP,ACTIVE}\sigma_{SMAP,ERA}}{\sigma_{ACTIVE,ERA}} \quad 3-6 \text{ b}$$

where  $\sigma_{SMOS}^2$ ,  $\sigma_{AMSR2}^2$ ,  $\sigma_{SMAP}^2$  are the data variances, and  $\sigma_{\varepsilon_{SMOS}}^2$ ,  $\sigma_{\varepsilon_{AMSR2}}^2$ ,  $\sigma_{\varepsilon_{SMAP}}^2$  are the errors variances.  $\sigma_{i,j}$  are data covariance, where  $i=SMOS, AMSR2, \text{ or } SMAP$ , and  $j=ACTIVE \text{ or } ERA$ .

The error variances  $\sigma_{\varepsilon_{SMOS}}^2$ ,  $\sigma_{\varepsilon_{AMSR2}}^2$ ,  $\sigma_{\varepsilon_{SMAP}}^2$  were used to estimate the merging parameters and for characterizing the errors of the merged product. Notice that these error estimates represent the average random error variance of the entire considered period, which is commonly assumed to be stationary. Furthermore, the soil moisture uncertainties of the target product (PASSIVE product) can also be determined from the error variances of single product.

### (3) Merging Passive Products

Except for the data merging period S1: 2007-June-01 to 2010-May-31 (AMSRE) and S3: 2011-Oct-04 to 2012-July-02 (SMOS), there are various combinations of data overlap as indicated in Figure 3.3. The data periods AMSRE and SMOS (S2: 2010-June-01 to 2011-Oct-03), SMOS and AMSR2 (S4: 2012-July-03 to 2015-March-30), SMOS, AMSR2, and SMAP (S5: 2005-March-31 to 2016-Dec-31) were merged by means of a weighted average on a pixel basis which considers the error properties of the individual data sets that are being merged. The method is the least squares method discussed in section 3.2.2, and the optimal weights for a weighted average are determined by the error variances of the input datasets. The error variances, which represent the rescaled error variances of rescaled data sets, have been calculated using triple collocation method as described before. The example specific equations used in merging period S5 can be presented as:

$$\omega_{SMOS} = \frac{\sigma_{\varepsilon_{AMSR2}}^2 \sigma_{\varepsilon_{SMAP}}^2}{\sigma_{\varepsilon_{SMOS}}^2 \sigma_{\varepsilon_{AMSR2}}^2 + \sigma_{\varepsilon_{SMOS}}^2 \sigma_{\varepsilon_{SMAP}}^2 + \sigma_{\varepsilon_{AMSR2}}^2 \sigma_{\varepsilon_{SMAP}}^2} \quad 3-7 \text{ a}$$

$$\omega_{AMSR2} = \frac{\sigma_{\varepsilon_{SMOS}}^2 \sigma_{\varepsilon_{SMAP}}^2}{\sigma_{\varepsilon_{SMOS}}^2 \sigma_{\varepsilon_{AMSR2}}^2 + \sigma_{\varepsilon_{SMOS}}^2 \sigma_{\varepsilon_{SMAP}}^2 + \sigma_{\varepsilon_{AMSR2}}^2 \sigma_{\varepsilon_{SMAP}}^2} \quad 3-7 \text{ b}$$

$$\omega_{SMAP} = \frac{\sigma_{\varepsilon_{SMOS}}^2 \sigma_{\varepsilon_{AMSR2}}^2}{\sigma_{\varepsilon_{SMOS}}^2 \sigma_{\varepsilon_{AMSR2}}^2 + \sigma_{\varepsilon_{SMOS}}^2 \sigma_{\varepsilon_{SMAP}}^2 + \sigma_{\varepsilon_{AMSR2}}^2 \sigma_{\varepsilon_{SMAP}}^2} \quad 3-7 \text{ c}$$

$$SM_{mS5} = \omega_{SMOS} SM_{SMOS} + \omega_{AMSR2} SM_{AMSR2} + \omega_{SMAP} SM_{SMAP} \quad 3-7 \text{ d}$$

where  $\omega_{SMOS}$ ,  $\omega_{AMSR2}$ ,  $\omega_{SMAP}$  are the relative weights of data sets SMOS, AMSR2, SMAP, and  $SM_{mS5}$  is the target merged product over S5. The method can also work in two datasets situation, such as merging period S2, the specific equations are presented below:

$$\omega_{AMSRE} = \frac{\sigma_{\varepsilon_{SMOS}}^2}{\sigma_{\varepsilon_{SMOS}}^2 + \sigma_{\varepsilon_{AMSRE}}^2} \quad 3-8 \text{ a}$$

$$\omega_{SMOS} = \frac{\sigma_{\varepsilon_{AMSRE}}^2}{\sigma_{\varepsilon_{SMOS}}^2 + \sigma_{\varepsilon_{AMSRE}}^2} \quad 3-8 \text{ b}$$

$$SM_{mS2} = \omega_{SMOS} SM_{SMOS} + \omega_{AMSRE} SM_{AMSRE} \quad 3-8 \text{ c}$$

where  $\omega_{SMOS}$ ,  $\omega_{AMSRE}$  are the relative weights of data sets SMOS, AMSRE, and  $SM_{mS2}$  is the target merged product over S2.

The weighted merging work in both three datasets case (S5) and two datasets case (S2, S4) as every single relative error variance against the ACTIVE and ERA has been determined. However, for certain locations, triple collocation analysis does not yield valid error estimates. In such cases, weights were equally distributed amongst the available sensors (e.g. 0.33 for AMSR2, SMOS, and SMAP over S5 if all three datasets are available, 0.5 for AMSRE and SMOS over S2, and 0.5 for AMSR2 and SMOS over S4). After the generation of merged data over S2, S4, and S5, and the scaled data over S1 and S3, the resulting consistent passive satellites product (hereafter is referred to as the PASSIVE product) was generated by concatenating these datasets based on the sequence of periods.

**3.3.2. Objective Blending**

After previous step *Satellite Data Merging*, the input datasets for *Objective Blending* include in-situ measured data, ERA-Interim data, merged PASSIVE, and ACTIVE data over blending period. The time range diagram is presented in Figure 3.5. The calibration period (the box with red borders) for surface soil moisture product is from Sept-2014 to Sept -2015 which aims to obtain the scaling parameters between in-situ measured surface soil moisture data and ERA-Interim soil moisture product. Then the parameters were used to scale ERA-Interim data over the entire period. The validation periods, which include one period form Sept-2015 to Sept-2016, and one period from Sept-2010 to Sept-2014, can test the quality of product under different merging situations.

Year	2007			2008			2009			2010			2011			2012			2013			2014			2015			2016								
Month	3	6	9	12	3	6	9	12	3	6	9	12	3	6	9	12	3	6	9	12	3	6	9	12	3	6	9	12	3	6	9	12	3	6	9	12
In-situ										Validation									Calibration			Validation														
ERA-Interim																																				
PASSIVE	AMSRE						SMOS+AMSRE			SMOS			SMOS+AMSR2									SMOS+AMSR2+SMAP														
ACTIVE																																				

Figure 3.6 Start-End Dates Diagram of all the Data Sets for Objective Blending

*Objective Blending* step aims to blend satellites data, reanalysis data and in-situ measured soil moisture datasets. Similar with *Satellites Data Merging*, the sub steps of *Objective Blending* include Rescaling, Error Characterization, and Merging as the Objective Blending flowchart presented in Figure 3.6. CDF matching explained in section 3.2.1 was used to constrain reanalysis dataset ERA-Interim with in-situ measured data climatology and to scale satellite data with rescaled reanalysis dataset. Triple collocation and least squares method were used to perform the error characterization and weighted average.

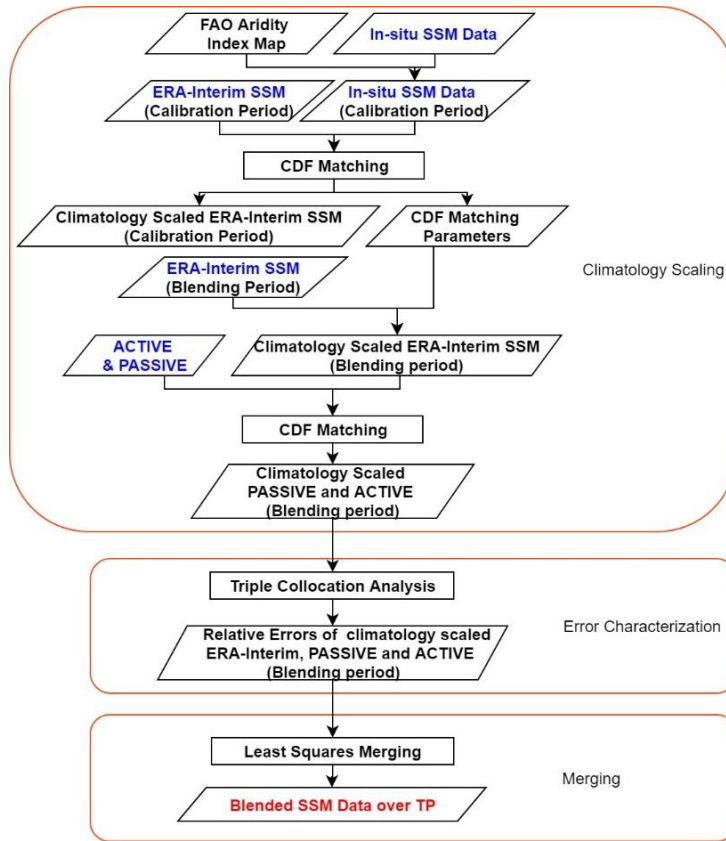


Figure 3.7: Objective Blending Flowchart

## (1) Rescaling

### i. In-situ Climatology

The in-situ soil moisture data climatology was obtained from the in-situ measured data over calibration period and the classification of the FAO Aridity Index map. The in-situ output datasets require a 25km spatial resolution to execute the next scaling step. The specific process to produce the data climatology was combining the in-situ data with the FAO Aridity Index map, for the calibration period between 01-Sep-2014 and 31-Aug-2015. After combining, it is comprehensible that the averaged in-situ measured soil moisture values of Naqu network are used to indicate the semi-arid situation, Maqu network for the sub-humid situation, and both Ali and Shiquanhe for the arid situation (Zeng et al., 2016). Each averaged value series was used to scale the reanalysis data ERA-Interim indicates different climate zones over Tibetan Plateau.

### ii. In-situ Climatology Scale ERA-Interim

First, ERA-Interim soil moisture products in 25km spatial resolution over the calibration period was scaled based on the obtained in-situ data climatology using CDF matching. The seasonal CDF matching parameters were obtained from it, and they were used in climatology scaling of ERA-Interim data in the blending period (2007-06-01 to 2016-12-31). Then, the climatology scaled ERA-Interim soil moisture data in 25km spatial resolution in blending period was produced using the CDF matching parameters obtained before. Also, the rescaling of reanalysis data ERA-Interim based on different seasons across the calibration period.

Table 3.1 Season separation from climatology scaling

Seasons	Month	Date
Winter	Dec-March	2010-12-01 to 2011-04-01
Transition 1	April	2011-04-01 to 2011-04-30
Monsoon	May-Oct	2011-05-01 to 2011-10-31
Transition 2	November	2010-11-01 to 2010-11-30

### iii. Rescaled ERA-Interim Scale Passive and Active Products

Execute another CDF matching between each merged satellite dataset (PASSIVE and ACTIVE) and the scaled ERA-Interim data generated from the previous step. The scaled ERA-Interim data over blending period was used to scale the PASSIVE product and the ACTIVE product which generated from the Satellite Data Merging section.

## (2) Error Characterization

The relative errors among the scaled PASSIVE, ACTIVE, and ERA-Interim, were calculated by using the Triple Collocation method as explained before. The results error variances  $\sigma_{PASSIVE}^2$ ,  $\sigma_{ACTIVE}^2$ , and  $\sigma_{ERA}^2$  were used to generate the optimal weights for objective blending. The equations are presented below:

$$\sigma_{\varepsilon_{PASSIVE}}^2 = \sigma_{PASSIVE}^2 - \frac{\sigma_{PASSIVE,ACTIVE}\sigma_{PASSIVE,ERA}}{\sigma_{ACTIVE,ERA}} \quad 3-9 \text{ a}$$

$$\sigma_{\varepsilon_{ACTIVE}}^2 = \sigma_{ACTIVE}^2 - \frac{\sigma_{ACTIVE,PASSIVE}\sigma_{ACTIVE,ERA}}{\sigma_{PASSIVE,ERA}} \quad 3-9 \text{ b}$$

$$\sigma_{\varepsilon_{ERA}}^2 = \sigma_{ERA}^2 - \frac{\sigma_{ERA,ACTIVE}\sigma_{ERA,PASSIVE}}{\sigma_{PASSIVE,ACTIVE}} \quad 3-9 \text{ c}$$

where  $\sigma_{PASSIVE}^2$ ,  $\sigma_{ACTIVE}^2$ ,  $\sigma_{ERA}^2$  are the data variances, and  $\sigma_{\varepsilon_{PASSIVE}}^2$ ,  $\sigma_{\varepsilon_{ACTIVE}}^2$ ,  $\sigma_{\varepsilon_{ERA}}^2$  are the errors variances.  $\sigma_{i,j}$  are data covariance, where  $i, j = \text{PASSIVE, ACTIVE, or ERA}$ .

## (3) Merging

A weighted average based on least squares method was used to merge scaled PASSIVE, ACTIVE, and ERA-Interim products. The equation for blending can be presented as:

$$SM_{blend} = \omega_{PASSIVE}SM_{PASSIVE} + \omega_{ACTIVE}SM_{ACTIVE} + \omega_{ERA}SM_{ERA} \quad 3-10$$

Where  $\omega_{PASSIVE}$ ,  $\omega_{ACTIVE}$ ,  $\omega_{ERA}$  are the relative weights of each soil moisture products. If  $\omega_{PASSIVE} + \omega_{ACTIVE} + \omega_{ERA} = 1$ , the merged estimation is unbiased optimal. The relative weights were calculated using the variance of satellites. The error variances of satellites calculated by using triple collocation, which used three collocated datasets to constrain the relative error variance determination without a manually decided reference. The equations to calculate the relative weights are presented as:

$$\omega_{PASSIVE} = \frac{\sigma_{\varepsilon_{ACTIVE}}^2 \sigma_{\varepsilon_{ERA}}^2}{\sigma_{\varepsilon_{PASSIVE}}^2 \sigma_{\varepsilon_{ACTIVE}}^2 + \sigma_{\varepsilon_{PASSIVE}}^2 \sigma_{\varepsilon_{ERA}}^2 + \sigma_{\varepsilon_{ACTIVE}}^2 \sigma_{\varepsilon_{ERA}}^2} \quad 3-11 \text{ a}$$

$$\omega_{ACTIVE} = \frac{\sigma_{\varepsilon_{PASSIVE}}^2 \sigma_{\varepsilon_{ERA}}^2}{\sigma_{\varepsilon_{PASSIVE}}^2 \sigma_{\varepsilon_{ACTIVE}}^2 + \sigma_{\varepsilon_{PASSIVE}}^2 \sigma_{\varepsilon_{ERA}}^2 + \sigma_{\varepsilon_{ACTIVE}}^2 \sigma_{\varepsilon_{ERA}}^2} \quad 3-11 \text{ b}$$

$$\omega_{ERA} = \frac{\sigma_{\varepsilon_{ACTIVE}}^2 \sigma_{\varepsilon_{PASSIVE}}^2}{\sigma_{\varepsilon_{PASSIVE}}^2 \sigma_{\varepsilon_{ACTIVE}}^2 + \sigma_{\varepsilon_{PASSIVE}}^2 \sigma_{\varepsilon_{ERA}}^2 + \sigma_{\varepsilon_{ACTIVE}}^2 \sigma_{\varepsilon_{ERA}}^2} \quad 3-11 \text{ c}$$

where  $\sigma_{\varepsilon_{PASSIVE}}^2$ ,  $\sigma_{\varepsilon_{ACTIVE}}^2$ , and  $\sigma_{\varepsilon_{ERA}}^2$  are the errors variances of satellites and ERA-Interim products.

They are relative errors represent the uncertainties of datasets while comparing with the others (Talagrand, 1997).

### 3.3.3. Depth Scaling

Year	2007			2008			2009			2010			2011			2012			2013			2014			2015			2016								
Month	3	6	9	12	3	6	9	12	3	6	9	12	3	6	9	12	3	6	9	12	3	6	9	12	3	6	9	12	3	6	9	12	3	6	9	12
In-situ surface SM													Validation						Calibration						Validation											
In-situ profile SM													Validation						Calibration						Validation											
Blended Surface SM	Blended Surface SM																																			

Figure 3.8: Input data for depth scaling

For depth scaling, an observation operator built by CDF matching method will be used to calculate profile soil moisture series from the blended surface soil moisture series. The Tibet-Obs in-situ measured surface and profile soil moisture datasets (Su et al., 2011) were used to generate this observation operator. As explained before, CDF matching was used to obtain the relationship between in-situ measured profile and surface soil moisture. Note that the profile soil moisture refers to a mean value of the soil moisture in the 0-80 cm depth:

$$\theta_p = \frac{2\theta_1 L_1 + (\theta_1 + \theta_2)L_2 + (\theta_2 + \theta_3)L_3 + \dots + (\theta_{i-1} + \theta_i)L_i}{2(L_1 + L_2 + \dots + L_i)} \quad 3-12$$

where  $i$  refers to the order of the soil layer;  $\theta_p$  is the profile soil moisture ( $\text{m}^3 \cdot \text{m}^{-3}$ );  $L_i$  is the soil layer depth (m);  $\theta_i$  is the  $i$ th layer soil moisture ( $\text{m}^3 \cdot \text{m}^{-3}$ ). The specific products used in the Tibet-Obs in-situ measured data include the soil moisture data of 5cm, 10cm, 20cm, 40cm, and 80cm under the land surface.

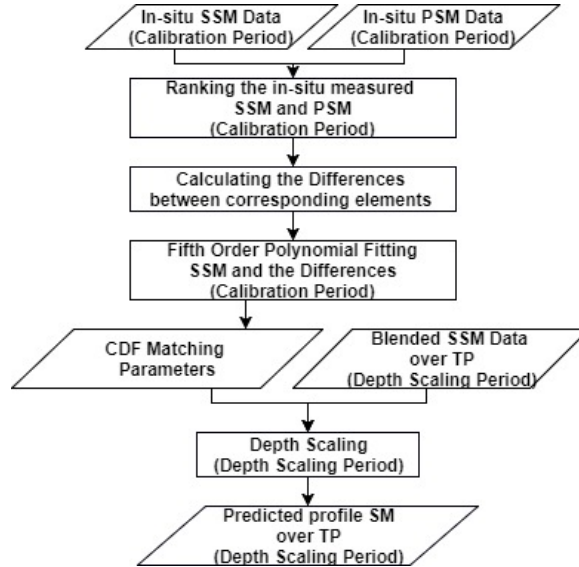


Figure 3.9: Depth Scaling Methodology Flowchart

As presented in the flowchart, the procedure of the depth scaling includes four steps. The first step was ranking the in-situ profile and surface soil moisture datasets over the calibration period. Then the differences between the corresponding values of profile and surface soil moisture were calculated as:  $\Delta = \theta_s - \theta_p$ . The third step was fitting a fifth-order polynomial to identify the relationship between the differences and surface soil moisture. To define the observation operators for depth scaling, Gao et al. (2016) identified the fifth-order polynomial as the optimal choice based on a pre-analysis. That is the reason why the fifth-order polynomial presented below was used to quantify the requested relationship:

$$\Delta' = k_0 + k_1 \times \theta_s + k_2 \times \theta_s^2 + k_3 \times \theta_s^3 + k_4 \times \theta_s^4 + k_5 \times \theta_s^5 \quad 3-13$$

where  $k_i$  ( $i = 1,2,3,4,5$ ) is the required parameter for depth scaling period and  $\Delta'$  is the predicted difference. The whole equation is the constructed observation operators. The target is scaling soil moisture data from surface to profile. The last step was rescaling the surface dataset using the predicted difference:

$$\theta'_p = \theta_s - \Delta' \quad 3-14$$

where  $\theta'_p$  is the predicted profile soil moisture (Gao et al., 2016).

## 4. RESULTS & DISCUSSION

### 4.1. Satellite Data Merging

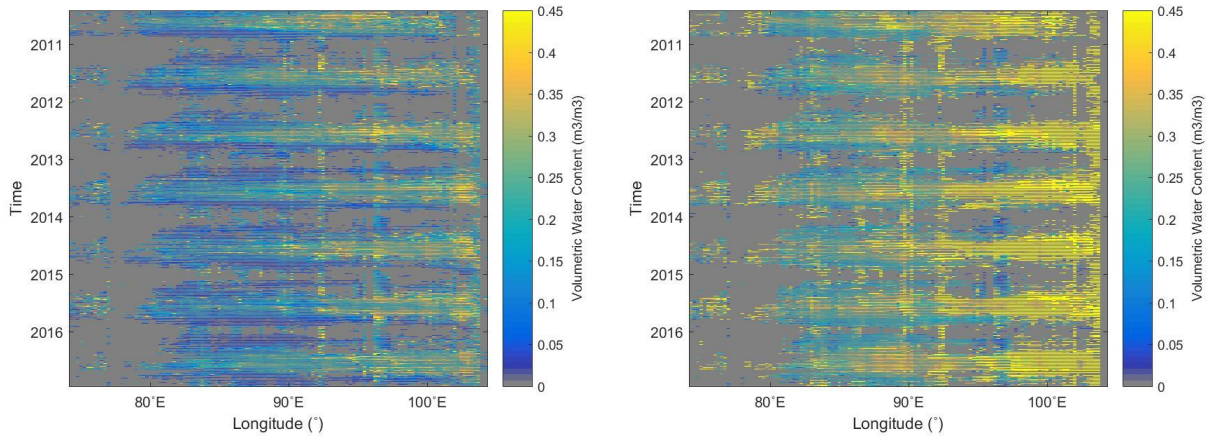
#### 4.1.1. Rescaling

The original SMOS soil moisture products have been scaled against the AMSR-E reference using the piece-wise linear cumulative distribution function (CDF) matching technique based on their overlapping period (S2: 01-June-2010 to 03-Oct-2011), the scaling parameters obtained in S2 were used to scale all the available SMOS products over the other periods (03-Oct-2011 to 31-Dec-2016). As the SMOS soil moisture product has a longest available period, the rescaled SMOS product in period S4 was used to scale AMSR2 data, and the rescaled SMOS products in period S5 were used to scale SMAP data. The detailed scaling procedure and the prepared datasets after rescaling is presented below in Table 4.1. The scaled SMOS 1 means the original SMOS data were scaled based on the AMSRE data over the same period directly, and the scaling parameters were generated in the meantime. The scaled SMOS 2 means the original SMOS data were scaled based on the parameters which generated in the SMOS scaling over S2.

Table 4.1 Prepared Datasets for Satellites Data Merging after Rescaling

	Original	Scaling Reference	Results
S1	AMSRE	\	AMSRE
S2	AMSRE	\	AMSRE
	SMOS	AMSRE	Scaled SMOS 1
S3	SMOS	Parameters	Scaled SMOS 2
S4	SMOS	Parameters	Scaled SMOS 2
	AMSR2	scaled SMOS 2	Scaled AMSR2
S5	SMOS	Parameters	Scaled SMOS 2
	AMSR2	scaled SMOS 2	Scaled AMSR2
	SMAP	scaled SMOS 2	Scaled SMAP

A latitude-time diagram can be used to demonstrate the average zonal dynamics, volumetric water content values in the diagrams mean the average soil moisture values along latitude. Figure 4.1 include latitude-time diagrams of both original and scaled SMOS datasets, which can serve as an example of rescaling. It is obvious that the rescaling step based on CDF matching method keeps the seasonal dynamics of the original products and changes the absolute values of original datasets (e.g. SMOS, AMSR2, and SMAP products). This conclusion has been demonstrated by Liu et al., (2011). The left side of the diagram indicates the western part of TP, which is relatively dry compared with the eastern part TP. The seasonal pattern of the eastern part TP is clear and regular. For example, soil moisture values are high during the monsoon season (May to October) and relatively low during winter (December to March). The grey areas in the diagram mean the data have been flagged out, especially the areas between 75°E to 80°E due to the desert area located in the western TP. Others, the absolute values of scaled SMOS data are higher than the original SMOS data, which means AMSRE products show relatively high soil moisture values. After scaling, they have consistent climatology now, which is a necessary condition for the following merging procedures.



(1) Original SMOS (2) Scaled SMOS  
 Figure 4.1: Longitude-Time diagram of Original and Scaled SMOS over the entire period (01-June-2010 to 31-Dec-2016)

**4.1.2. Error Characterization**

Based on the discussion in section 3.3.1, several procedures were performed to test the feasibility of triple collocation method. In this section, the processing procedures over S5 (31-Mar-2015 to 31-Dec-2016) serve as examples. Figure 4.3 and Figure 4.4 shows the triplets number and the relative errors over merging period S5. It should be emphasized that the triplets number in Figure 4.2 means the number of three-collocated data with ACTIVE and ERA-Interim, while the number of pixels has relative errors in Figure 4.3 indicates that these pixels can give a valid error variance after performing a triple collocation analysis. However, as it presented in Figure 4.3, it is evident that the error variances of many pixels cannot be decided, where only the equal weight average can be performed to merge the datasets.

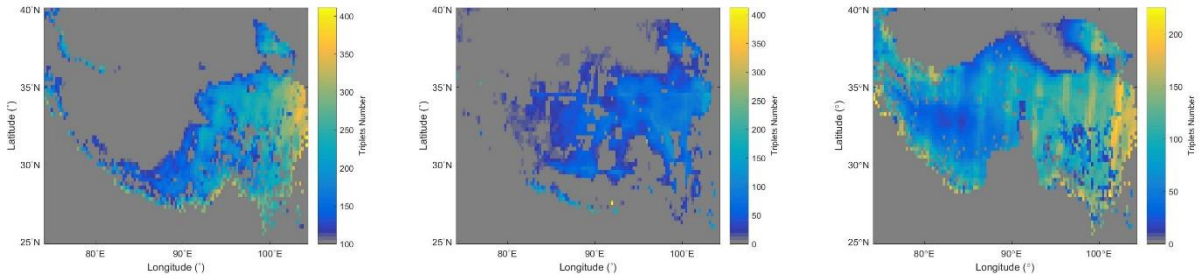


Figure 4.2: Triplets Number of Scaled AMSR2, SMOS, and SMAP over Merging Period S5 (31-Mar-2015 to 31-Dec-2016)

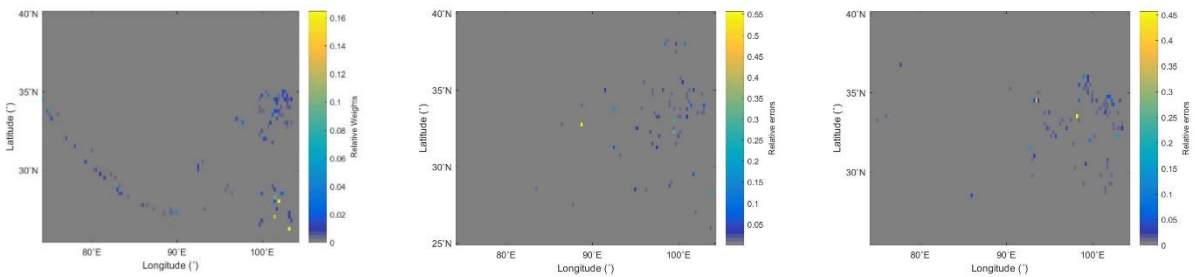


Figure 4.3: Relative errors of Scaled AMSR2, SMOS, and SMAP over Merging Period S5 (31-Mar-2015 to 31-Dec-2016)

For other satellites data merging period, the error characterisation procedures are similar. For S1 and S3, as only one satellites data exists, the relative errors are calculated to characterise the relative uncertainties without another purpose. For S2, the merging time is relatively short, and the data number of SMOS is much less than AMSRE, but these conditions did not influence the performance of error characterisation. For S4, the relative errors of SMOS and AMSR2 are similar. The specific averaged values of them over the merging period and the entire study area are presented below in Table 4.2.

Table 4.2 Averaged Relative Errors of Satellites Data over every Merging Periods

Period	Date	Averaged Relative Errors (m <sup>3</sup> / m <sup>3</sup> )		
S1	2007-06-01 to 2010-05-31	AMSRE 0.0023		
S2	2010-06-01 to 2011-10-03	AMSRE 0.0031	SMOS 0.0068	
S3	2011-10-04 to 2012-07-02	SMOS 0.0231		
S4	2012-07-03 to 2015-03-30	SMOS 0.0085	AMSR2 0.0057	
S5	2015-03-31 to 2016-12-31	SMOS 0.0074	AMSR2 0.0047	SMAP 0.0065

#### 4.1.3. Merging

The final averaged merging weights of satellites data are presented in Table 4.3. In merging period S1 and S3, only one satellite data comprised in the merged product, so, the merging weights of them is 1. Others, the merging weights were calculated from relative errors indicated in Figure 4.4 and table 4.2, the pixels without valid relative errors were set the equal weights. So, the averaged merging weights in table 4.3 indicate the averaged weights include the equal weights situation. As AMSRE and AMSR2 have lower errors, the weights of them are relatively high, and SMOS, SMAP has similar relative errors which are higher than AMSRE and AMSR2, the weights of them are relatively low. However, the difference is small, especially in S5. The difference between the merging results of this method and the simple averaged merging are small, but the uncertainties of the merged products are reduced. Figure 4.4 presents an example of passive satellites data merging, which is a merging of scaled AMSR2, scaled SMOS, and scaled SMAP. The result merged PASSIVE product shows a spatial extension of surface soil moisture data.

Table 4.3 Averaged Merging Weights of Satellites Data over every Merging Periods

Period	Date	Averaged Merging Weights		
S1	2007-06-01 to 2010-05-31	AMSRE 1		
S2	2010-06-01 to 2011-10-03	AMSRE 0.613	SMOS 0.387	
S3	2011-10-04 to 2012-07-02	SMOS 1		
S4	2012-07-03 to 2015-03-30	SMOS 0.431	AMSR2 0.569	
S5	2015-03-31 to 2016-12-31	SMOS 0.313	AMSR2 0.395	SMAP 0.292

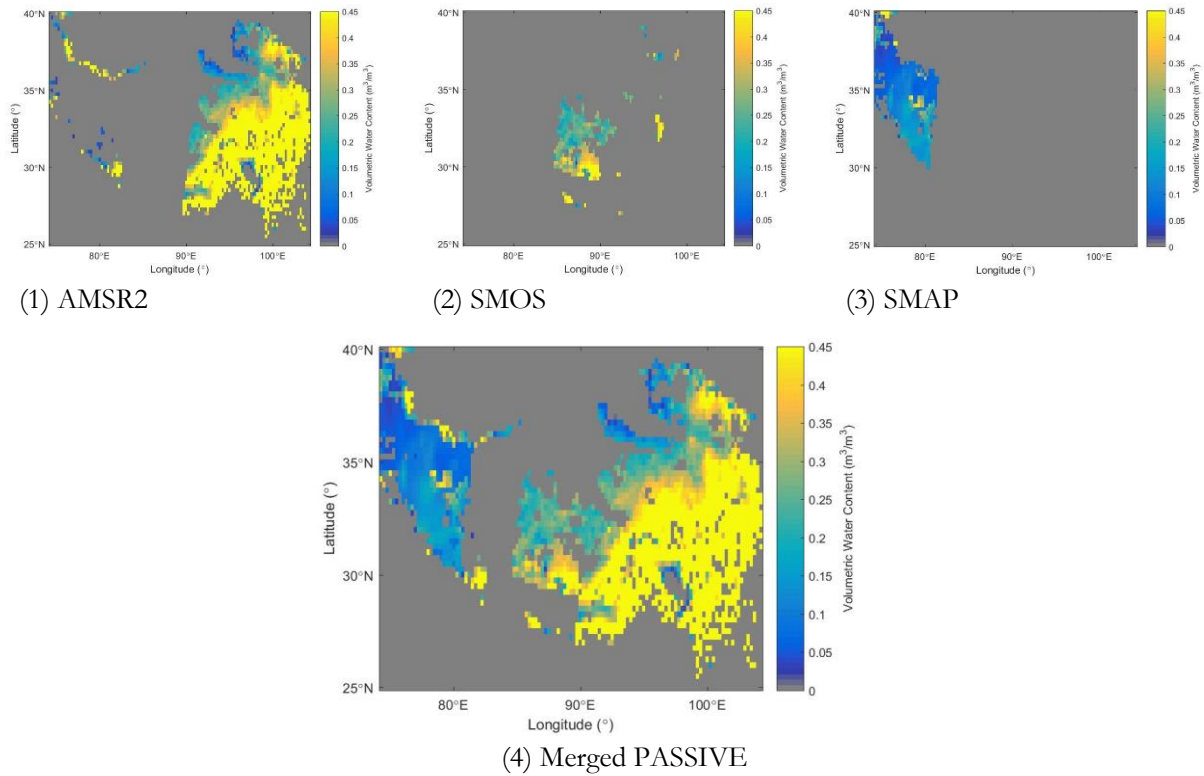


Figure 4.4 Satellites Data Merging example on 05-June-2016

where: (1) scaled AMSR2 soil moisture data (2) scaled SMOS soil moisture data (3) scaled SMAP soil moisture data (4) Merged PASSIVE soil moisture data

## 4.2. Objective Blending

### 4.2.1. Climatology Scaling

The first climatology scaling was performed to scale ERA-Interim products with the in-situ climatology. There were two sub-steps to perform the ERA-Interim climatology scaling as explained in section 3.3.2. First, scale the original ERA-Interim soil moisture data based on the in-situ data climatology, for the calibration period between 1-Sept-2015 and 31-Aug-2016. Then the CDF matching seasonal parameters generated during the calibration period were used to scale the ERA-Interim products over the entire period (Blending period: 2007-June-01 to 2016-Dec-31). The time-longitude diagram for the original ERA-Interim and the scaled ERA-Interim are presented below, as well as an example CDF curves figure to illustrate how the CDF matching worked. The time-longitude diagrams were used to investigate the calibration results (Zeng et al., 2016). They can show the temporal evolution of the zonal average of soil moisture data along the longitude across the Tibetan Plateau (from west to east).

As presented in Figure 4.5 (3), the original ERA-Interim did not show obvious seasonal change while it is significant in the in-situ climatology (Figure 4.5 (1)). For example, the eastern part of Tibetan Plateau, it is dry during the winter, and it is wet during the monsoon season. Moreover, the western part is relatively dry when compared with eastern part. After being scaled by using the CDF matching method, the scaled ERA-Interim product shows a similar pattern to the time-longitude diagram of in situ climatology. The volumetric water content is around  $0.35 (m^3/m^3)$  during the wet season (monsoon season: from May to October), while it is around  $0.07 (m^3/m^3)$  during the dry season (winter: from December to March). And also, they have two transition seasons (April and November).

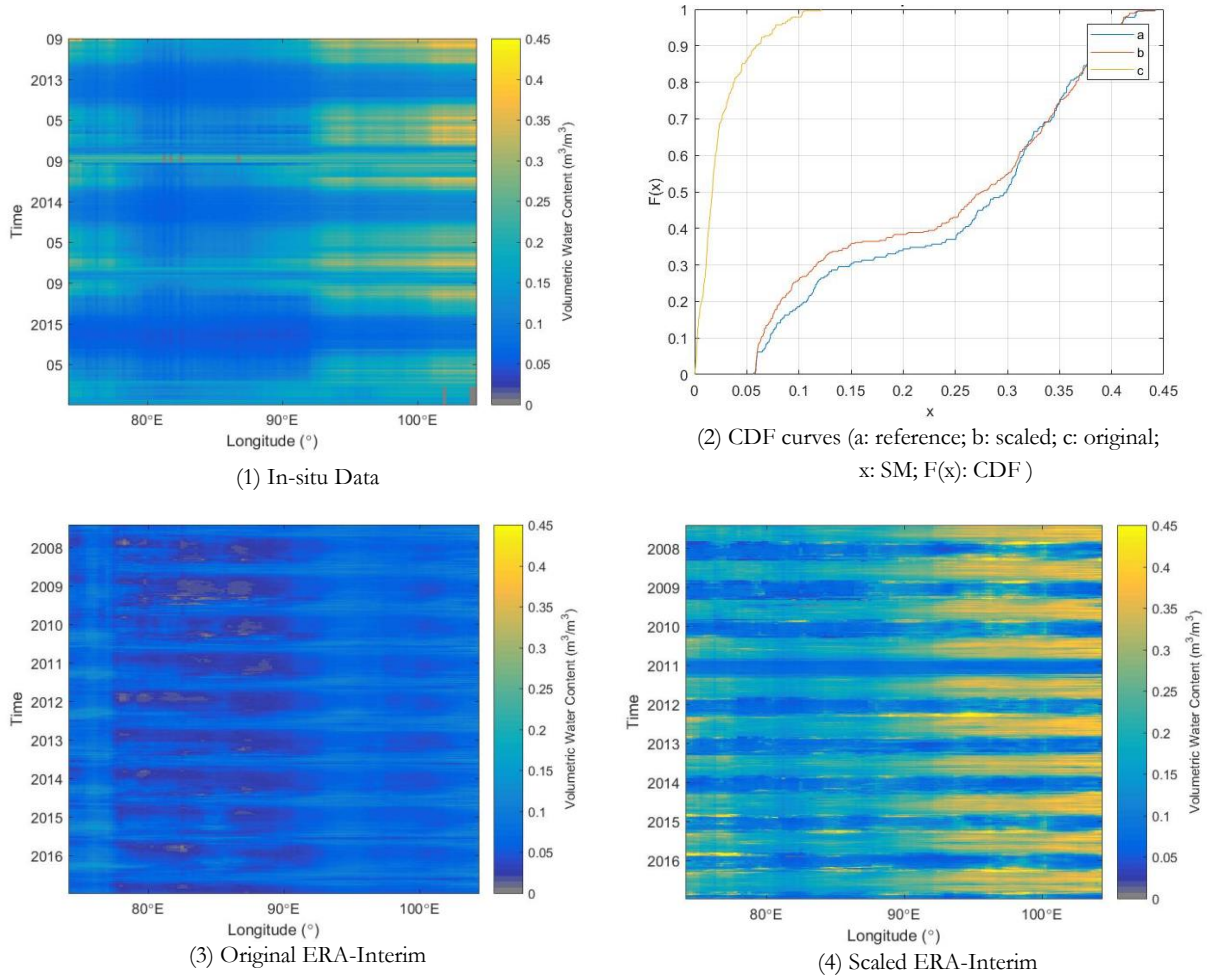


Figure 4.5: Example Curves of CDF Matching and Time-longitude Diagrams of SM products (1) In-situ data climatology; (3) original ERA-Interim data over the entire period; (4) ERA-Interim data after scaling based on in-situ climatology

Then, the rescaled ERA-Interim soil moisture product was used to scale the PASSIVE and ACTIVE products. The time-longitude diagrams of original and scaled PASSIVE and ACTIVE products and also the reference data: scaled ERA-Interim data presented in Figure 4.6. Although the original PASSIVE and ACTIVE products have some spatial-temporal patterns, which can reveal the seasonal and spatial dynamics, they are not significant. Moreover, both of them overestimated the soil moisture over Tibetan Plateau, especially during the monsoon seasons. After scaling, both AMSRE and ASCAT data show a similar climatology with the scaled ERA-Interim data, as well as the dynamic range of soil moisture. The effect of climatology scaling was relatively significant, and the averaged soil moisture in the eastern part of Tibetan Plateau was up to  $0.45(m^3/m^3)$  before scaling. After scaling, the absolute values of PASSIVE products changed based on the systematic difference with the reference data (scaled ERA-Interim). Others, in original ACTIVE products, the western part of Tibetan Plateau show a relative high value, while it is reduced during the climatology scaling. The time series of PASSIVE and ACTIVE products scaling in Figure 4.6 and 4.7 are revealing a similar conclusion.

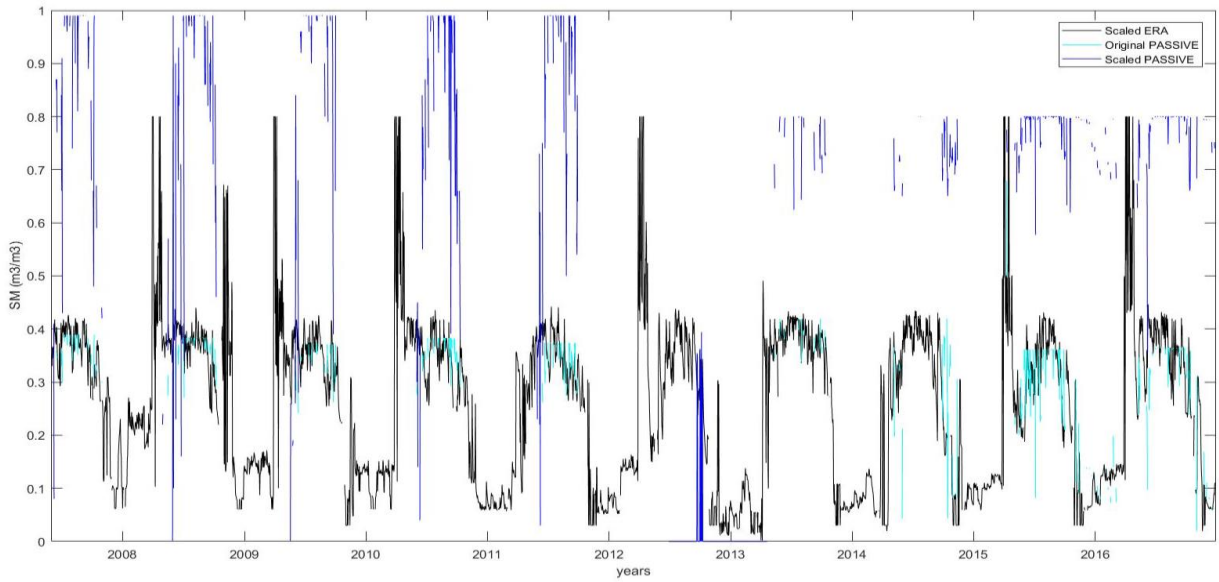


Figure 4.6: Time series of scaled ERA-Interim, original and scaled PASSIVE products.

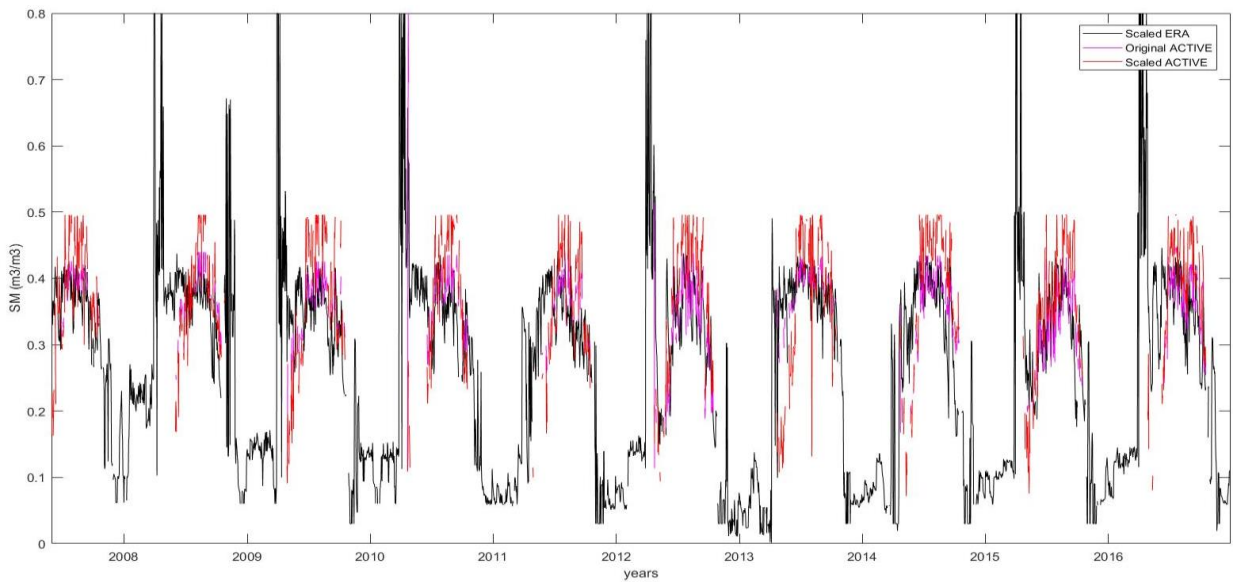


Figure 4.7: Time series of scaled ERA-Interim, original and scaled ACTIVE products.

#### 4.2.2. Blending

The scaled PASSIVE, ACTIVE, and ERA-Interim soil moisture products with the consistent climatology blended into one consistent set of soil moisture data using the objective blending method introduced in section 3.3.2. Figure 4.8 (4) presents the spatial-temporal dynamics of blended surface soil moisture product, which indicates that blended soil moisture product is systematically close to the scaled ERA-Interim. So, it is close to the in-situ climatology as well.

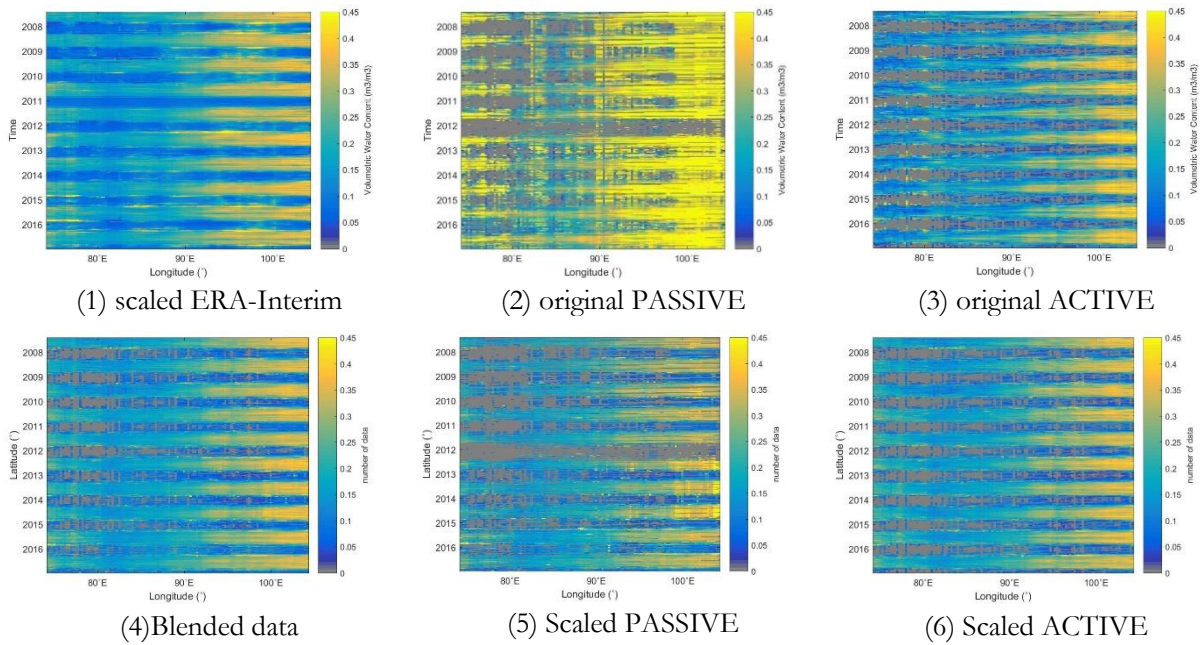


Figure 4.8: Time-longitude Diagrams of SM Products

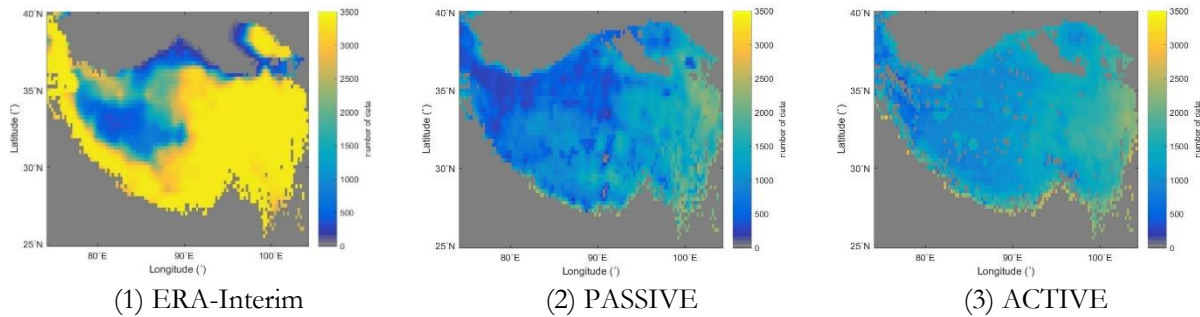


Figure 4.9: Data Number Map

The blending of these scaled soil moisture products implemented with two sub-steps. First, blend the three collocated SM data, where the datasets can form triplets together. Second, blend the rest of data, where one satellite data collocates individually with the scaled ERA-Interim data, but not collocate with another satellite data to form triplets. To tackle the first situation, I checked the data number of each product and the constructed triplets number first. The data number maps in Figure 4.9 aim to give a general idea of the data number magnitude, which influences the decision of suitable triplets' number and the analysis of statistics. The ERA-interim product has more than 3500 data across the southern and eastern part of Tibetan Plateau, and even have many data in the arid zones. The PASSIVE and ACTIVE products have less data number, but they are better distributed, mainly in ACTIVE.

Then I checked the triplets number, which indicates the number of three-collocated data. Figure 4.10 (1) presents the amount of collocated SM data among the three datasets over the blending period, and it shows that the eastern areas have around 1200 triplets while some western regions have less than 400 triplets. Considered the original data number, the three-collocated data are less than half of them. Also, in figure 4.10(1), only the data with more than 100 observation triplets were presented as 100 observation triplets are required for a reliable estimation of the relative error among the three SM products(Zwieback et al., 2012).

Next, the minimum correlation coefficient among the three collocated soil moisture products was calculated to check if the identified number of triplets is statistically significant to apply with triple collocation method. The distribution of minimum correlation coefficient presented in figure 4.10 (2) and most of the areas are with a minimum correlation coefficient more than 0.15, which is required for a sample with more than 100 data to achieve the statistical significance.

Figure 4.10 (3) plotted with (1-P\_values), which shows the significance level corresponding to the minimum correlation coefficient and indicates that the area with triplet number >100 (where the  $p\_value < 0.05$ ) are all statistically significant to be applied with TC method to identify the relative errors. As most of the P\_values were close to zero, the 1-P\_values plot improved the visibility of the image.

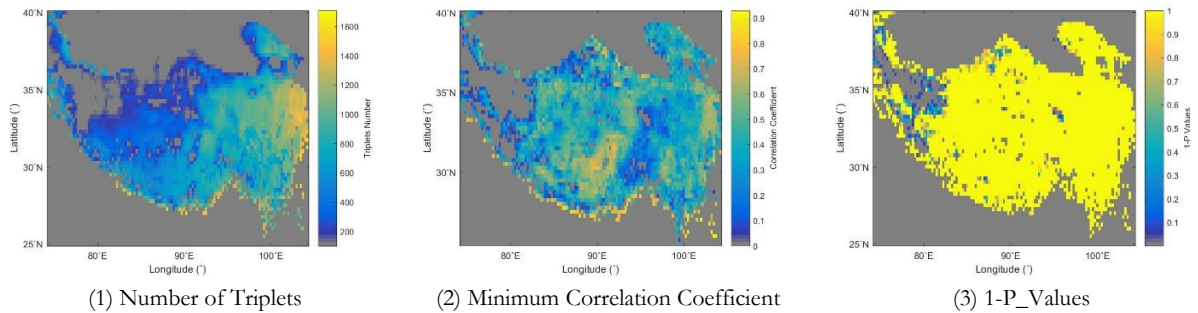


Figure 4.10 Statistics of triple collocated data

Figure 4.11 shows the optimal weights of scaled ERA-Interim, PASSIVE and ACTIVE, which determined by least squares and triple collocation method. Among three soil moisture products, the ACTIVE has the smallest average relative error (0.0032  $\text{cm}^3/\text{cm}^3$ ) while the highest weight (0.5999) contributing to the blended products. The average weight of the PASSIVE product is 0.1402, and for ERA is 0.2999. The reason why the merging weights of PASSIVE are relatively low is the low soil moisture retrieval rate of passive satellites over the central and western TP. The AMSRE flagged out the region with frozen ground, which leads to the low soil moisture retrieval rate of passive microwave satellites. Such a limitation caused by the problem of distinguishing the dry and frozen soil using passive satellites observations (Wolfgang Wagner et al., 2013).

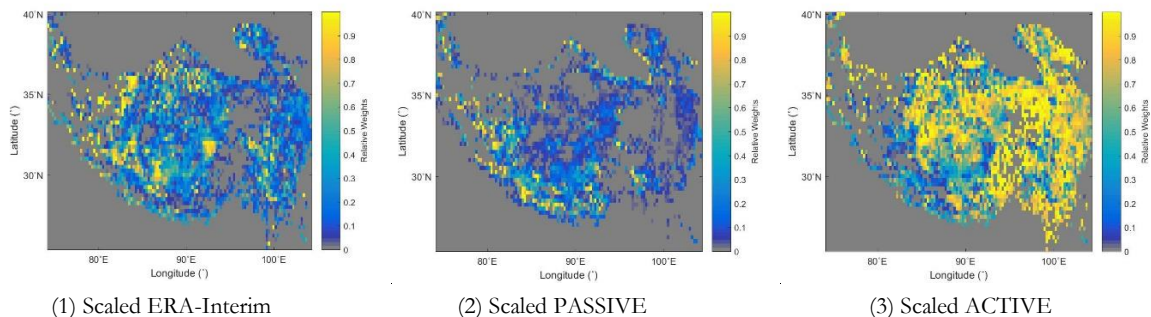


Figure 4.11: Optimal weights of soil moisture products

The second step is to blend the scaled satellite SM data collocating individually with the scaled ERA-Interim data, but not collocating with each other. The weights for blending determined from the scaled PASSIVE product and ERA-Interim, or the scaled ACTIVE product and ERA-Interim. For those two arranged PASSIVE data (no ACTIVE data satisfied the requirement in this case), the average weight of

ERA-Interim is 0.45981, and the average weight of the scaled PASSIVE is 0.54032, corresponding with a relative error of  $0.01231 \text{ cm}^3/\text{cm}^3$  and  $0.0063 \text{ cm}^3/\text{cm}^3$ , respectively. As can be seen from Figure 4.12, both the scaled PASSIVE and ACTIVE blended into the final SM product after *objective blending*.

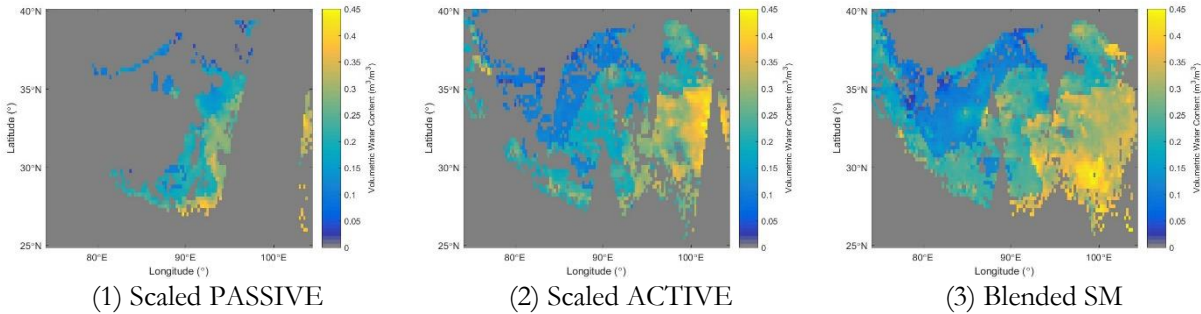


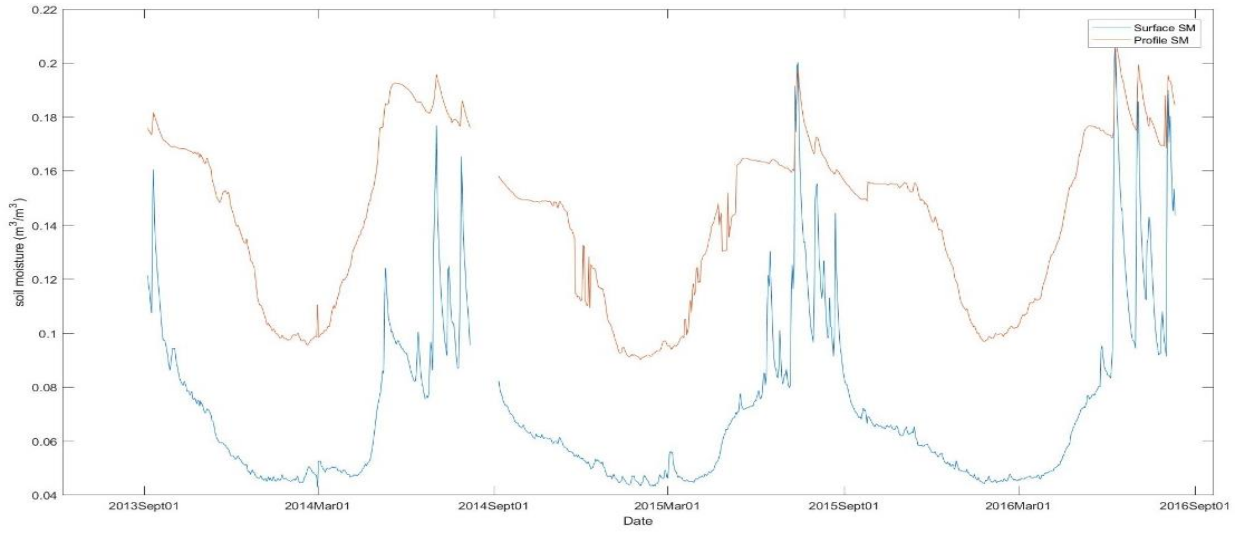
Figure 4.12: Soil Moisture data on 05-June-2007

### 4.3. Depth Scaling

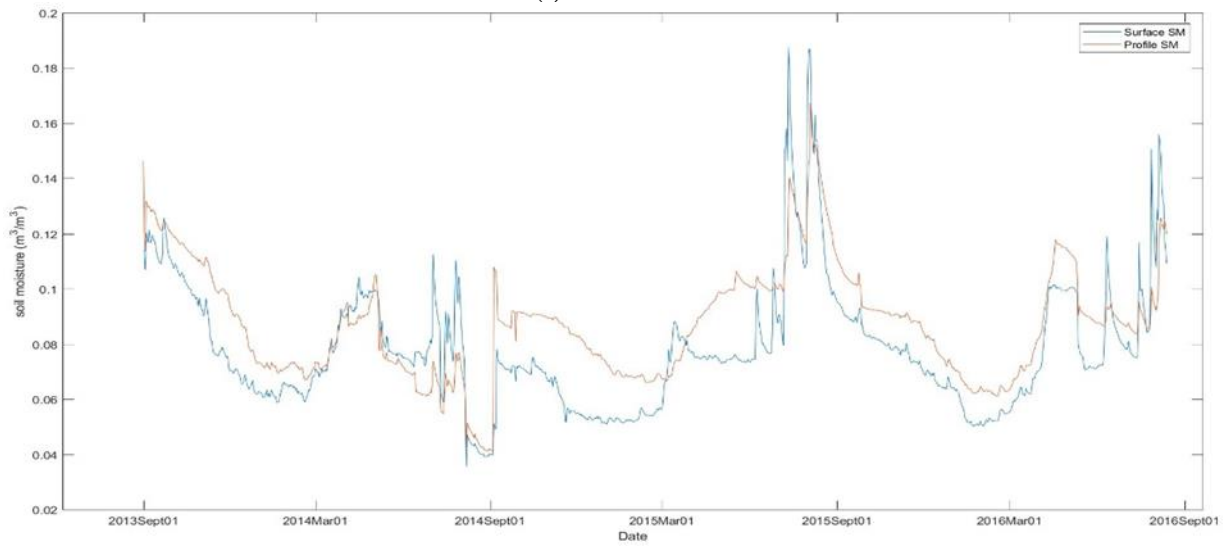
#### 4.3.1. Calibration

The calibration of depth scaling aims to generate an observation operator to define the relationship between the surface-profile difference and the surface soil moisture. The observation operator means one fifth order polynomial for one single grid to illustrate the relationship between the time series of profile soil moisture and surface soil moisture. First, the in-situ measured surface and subsurface soil moisture over four different networks were studied. The observation operators generated from the Ali and Shiquanhe networks represented Arid climatic zones. The relationships found in Naqu network and Maqu network serve Semiarid zone and Subhumid area individually. In Ali, there are four stations for soil moisture measuring, and the zonal averaged surface and subsurface (5cm, 10cm, 20cm, 40cm, and 80cm) soil moisture time series attached in the appendix.

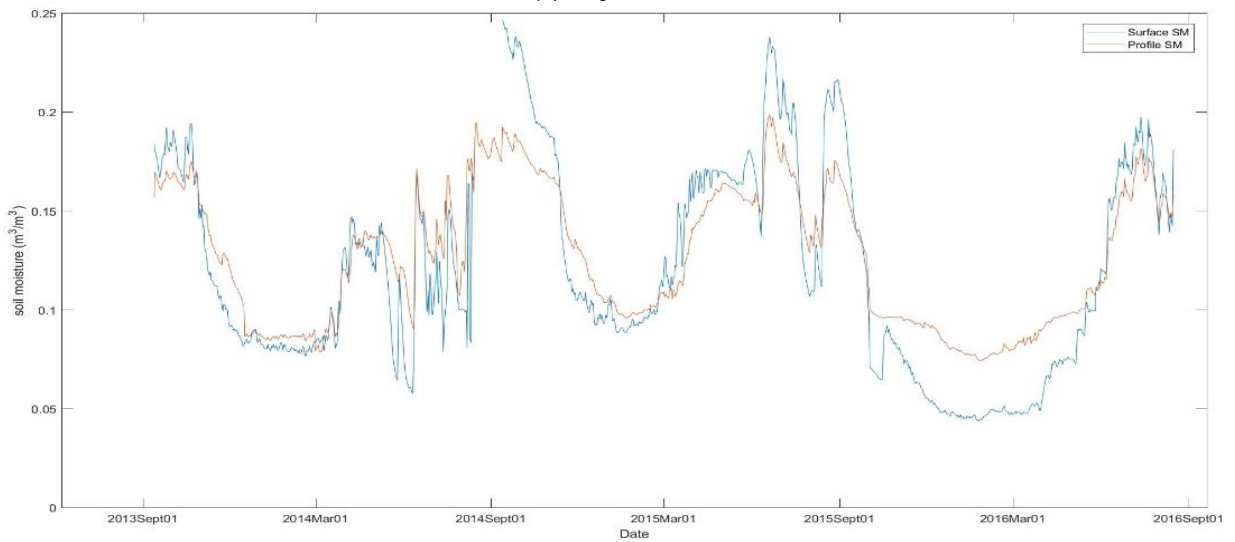
The relationship between surface and subsurface soil moisture is complicated. First, look into the time series of zonally averaged surface soil moisture and profile soil moisture presented in Figure 4.13. The time series in Figure 4.13 (1) is the averaged soil moisture conditions from 4 stations in Ali network. The profile soil is wetter than a surface with a smaller fluctuation. However, when it refers to a single station, sometimes there are incredibly high soil moisture values in 80cm soil layer, and some stations, the 40cm soil layer have an extremely high value, and in 80cm the moisture values come down sharply. So, the way to generate the averaged values is averaging soil moisture layer by layer instead of averaging station by station. Then, the soil moisture values presented below were used to generate the observation operators using CDF Matching method.



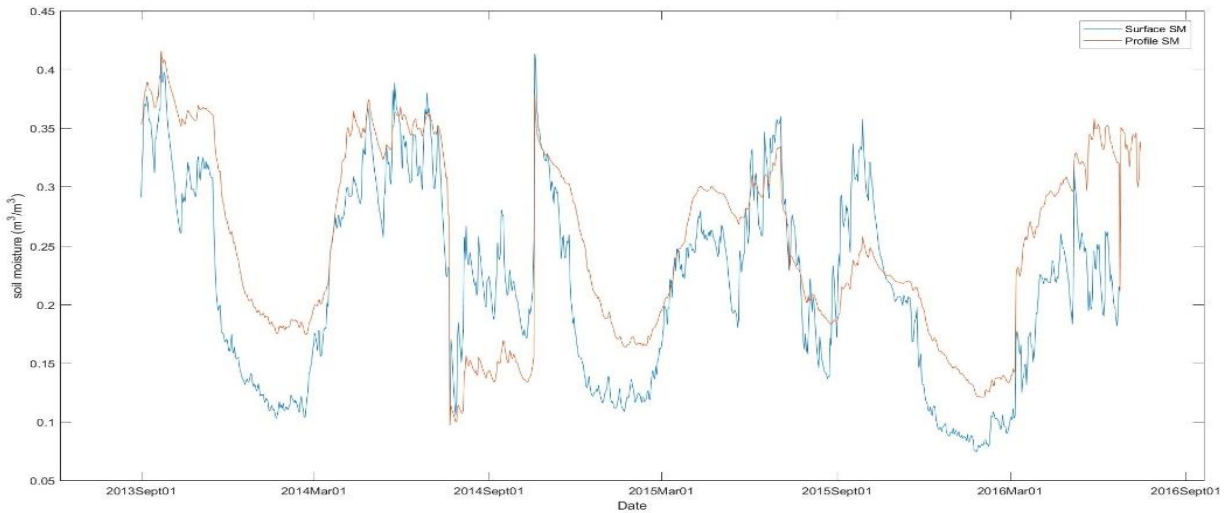
(1) Ali Network



(2) SQ Network



(3) Naqu Network

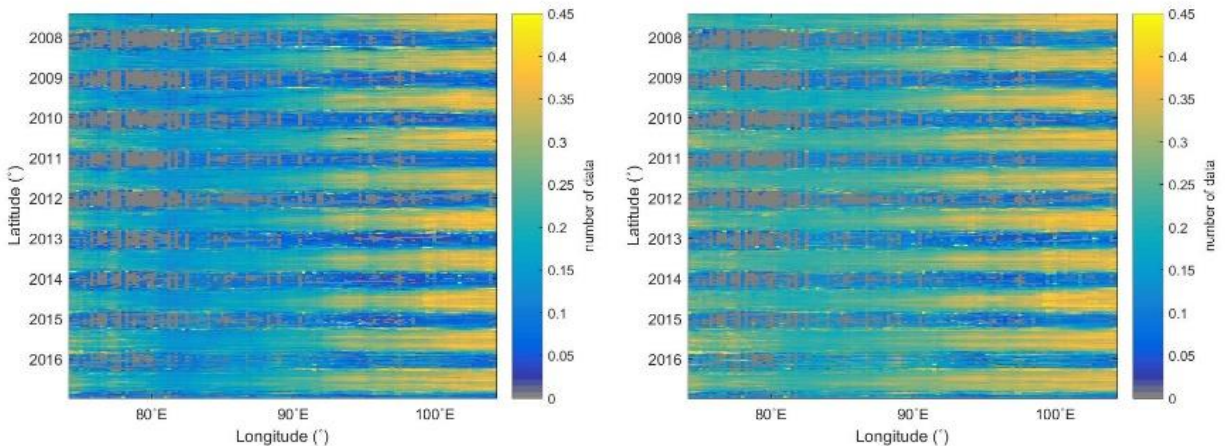


(4) Maqu Network

Figure 4.13 In-situ Measured surface and subsurface SM Data over Calibration Period (01-Sept-2013 to 31-Aug-2015)

### 4.3.2. Scaling

After calibration, the observation operators of different climatic zones scaled every single grid over the entire study period (01-June-2007 to 31-Dec-2016). The scaling results presented in the time-longitude diagrams. The Figure 4.14 (1) shows the spatial-temporal dynamics of blended surface soil moisture data which generated in previous section 4.2. It is a consistent surface soil moisture product, and it can serve as a single dataset to be studied. The seasonal dynamics of it is apparent that during wet monsoon season, the surface soil moisture data may reach  $0.4 (m^3/m^3)$  in subhumid regions, and during the winter, the surface soil moisture is extremely dry or frozen. The seasonal differences are low in semiarid areas and is obvious in subhumid and arid regions. The Figure 4.14(2) shows the spatial-temporal dynamics of scaled profile soil moisture obtained in this section. Compared with the time series in Figure 4.13, there are some similar patterns exist. For example, in arid regions, the profile soil moisture is slightly higher than surface which is obvious in figure 4.13(1). In Figure 4.14(2), the soil moisture values in arid region are slightly higher than surface and the seasonal difference are relatively small. Others, the semiarid area shows a smoother pattern which means the fluctuation is smaller, but the absolute values are slightly higher than surface. The profile product shows a reasonable pattern and kept the in-situ data climatology qualitatively.



(1) Surface SM

(2) Profile SM

Figure 4.14: Time-longitude Diagrams of Depth Scaling Reference and Results

## 5. DISCUSSION

The main output of this research includes the blended surface soil moisture product and the profile soil moisture. The discussion about these products includes the anomalies analysis and inter-comparison with other products.

### 5.1. Surface Soil Moisture

The homogenised and merged product presents surface soil moisture with global coverage and a spatial resolution of 0.25°. The time spans the entire period covered by the individual sensors, i.e. 2007-2016, while measurements are provided at a 1-day sampling.

#### (1) Anomalies of Blended data

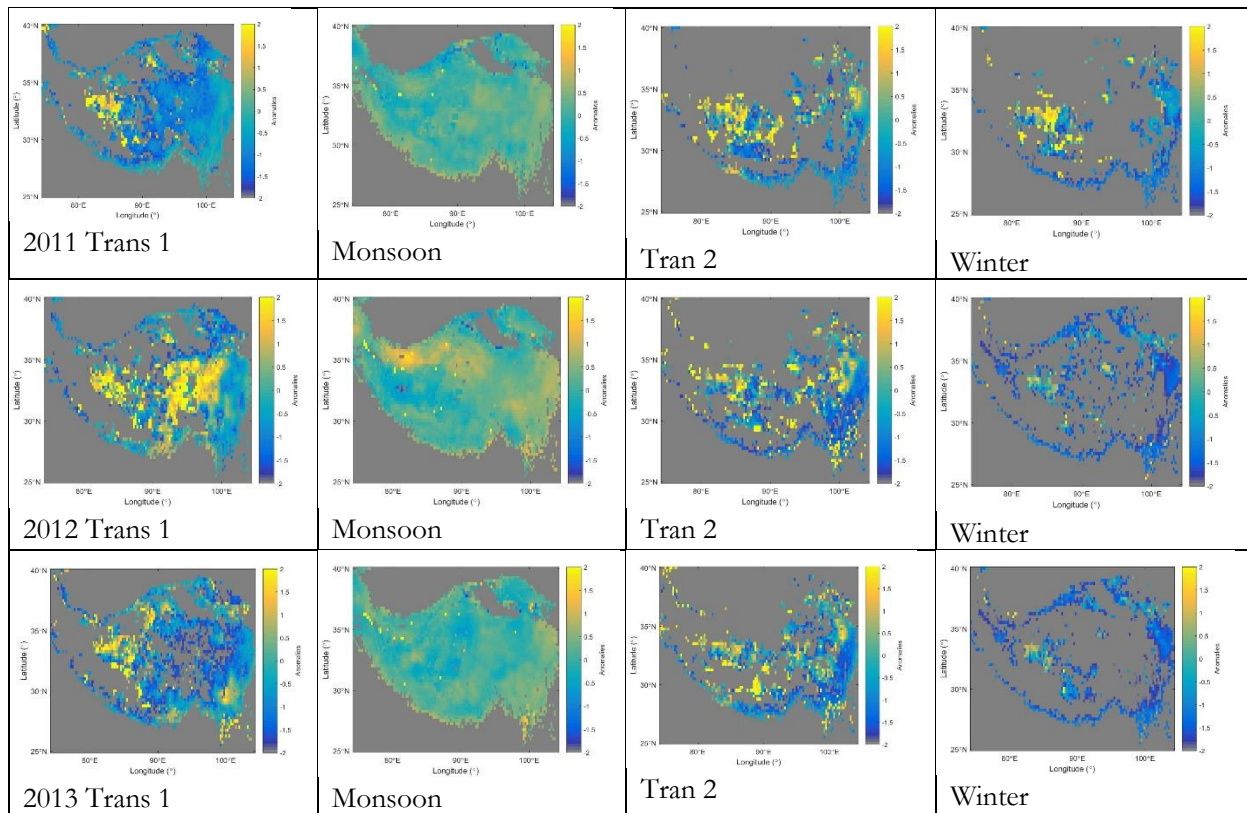


Figure 5.1 Anomalies of Profile Soil Moisture

The anomaly is a dimensionless value shows the seasonal pattern of soil moisture time series. In anomalies series, the negative values represent the dry condition, and the positive values represent the wet condition. In Figure 5.1, the anomalies plot in four seasons of three years, where the Trans indicate transition period. The anomalies are relatively gentle when compared with the other seasons during the monsoon season, and the anomalies values are close to zero, which means the soil moisture condition is close to the systematic mean. In the winter, the anomalies are negative in the eastern part which means that the soil in the subhumid area is dry during winter. However, in the centre of the Tibetan Plateau, the anomalies become positive, which means the soil is wet during the winter. Moreover, in the transition period, the anomalies of the centre Tibetan Plateau are high while the other place is drier than the average.

**(2) Inter-comparison**

In this section, I compared the blended SM with different SM products for the blending period between 1-Sept-2015 and 31-Aug-2016. The in-situ measurements over Tibet-Obs networks (Naqu, Maqu, Ali, and Shiquanhe) were served as a reference to validate the results product. In Figure 5.2, the original soil moisture products include SMOS, AMSR2, SMAP, ERA-Interim, PASSIVE, ACTIVE and their corresponding scaled SM data. The Taylor diagram represents the correlation coefficient, the centred unbiased root-mean-square difference, and the standard deviation using a two-dimensional plot (Petropoulos, 2013). Also, in figure 5.2, an arithmetic average was performed to obtain the average value of original data and scaled data.

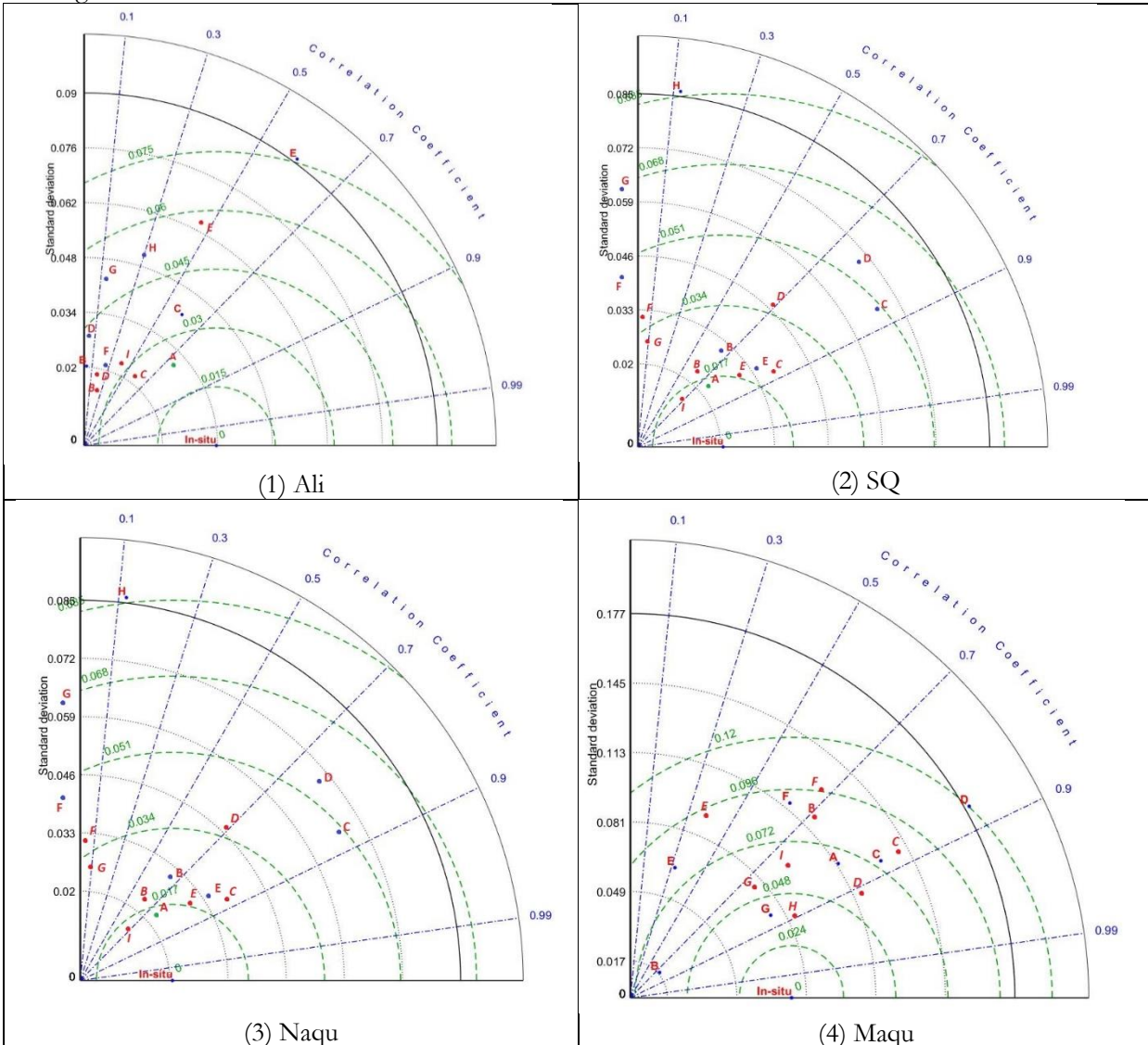


Figure 5.2 Taylor Diagram: Inter-comparison between Blended Data and Others

The arithmetic averaged values H, and I represent the averaging of original soil moisture data and the averaging of the scaled soil moisture data. Compared I with the blended data A, the least squares method performs better than arithmetic averaging in Ali an SQ networks, which is closer to the in-situ measured data with a similar correlation coefficient and root mean squares. Although they perform similar effect in Maqu, it still verified that the least squares method is needed and performed better in the arid areas over Tibetan Plateau.

The original satellites data and merged PASSIVE, merged ACTIVE data (B: SMOS; C: AMSR2; D: SMAP; E: ERA-Interim; F: PASSIVE; G: ACTIVE) have higher standard deviations before scaling. The greater standard deviation indicates the more fluctuations, especially for PASSIVE and ACTIVE. After a scaling based on the in-situ climatology, the standard deviation of them became smaller. It is one of the reasons why a climatology scaling is needed before a merging step. It is important to eliminate the systematic difference between different datasets before the further merging can perform, and the climatology scaling performs well.

The PASSIVE and ACTIVE products did not perform well before climatology scaling, while SMOS and AMSR2 performed well in most of the conditions. The SMOS data estimated soil moisture accurately and captured the in-situ surface soil moisture dynamics. Especially in SQ and Naqu network, it performs similarly to the blended data. Others, when compared PASSIVE and ACTIVE, the scaled ACTIVE performs better, which means the average weight of ACTIVE is greater than the weight of PASSIVE in the Blended product.

### 5.2. Subsurface Soil Moisture

The analysis methods are similar to the blended data analysis. The anomalies analysis will be carried out over the scaled period. The inter-comparison operated with SMAP L4 profile soil moisture data and the module simulated profile soil moisture data (i.e. GLDAS, ERA-Interim).

#### (1) Anomalies of Profile Soil Moisture

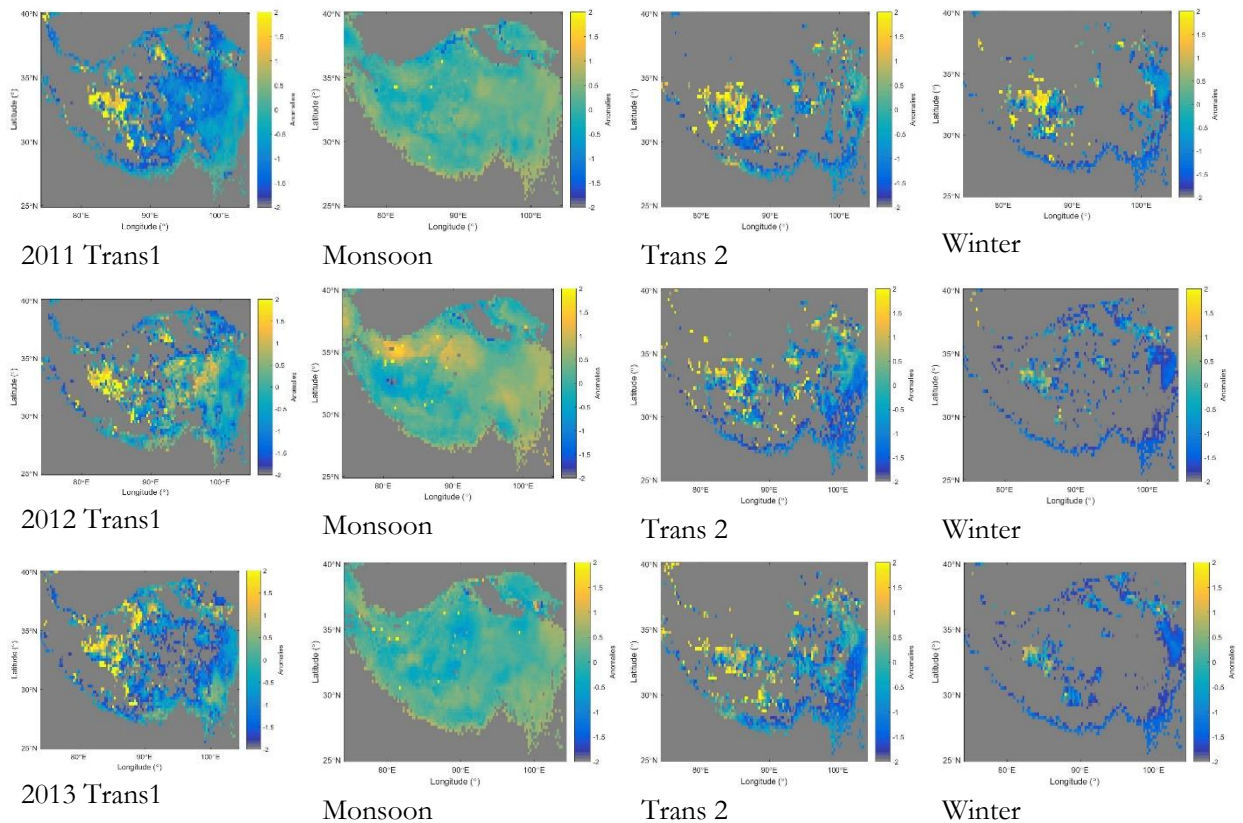


Figure 5.3 Anomalies of Profile Soil Moisture

In the validation period, anomalies show similar seasonal dynamics. As the positive anomalies indicate a wet condition, while the negative one indicates dry, the Monsoon season is wet and with a small vibration when compare with winter, or the transition time. The general pattern of the anomalies distribution is similar to the anomalies of blended surface product. The CDF Matching performed to scale surface soil moisture data aims to eliminate the systematic differences, which would influence the mean value. The mean value then influences the anomalies characteristic. In the middle of the Tibetan Plateau, the anomalies values are more positive than surface data, which means wetness kept procedure during the winter in arid and cold areas.

**(2) Inter-comparison**

The inter-comparison of profile soil moisture data include the comparison with B: ERA-Interim profile soil moisture data; C: GLDAS profile soil moisture data; D: SMAP L4 profile soil moisture data. Moreover, also the corresponding in-situ scaled data.

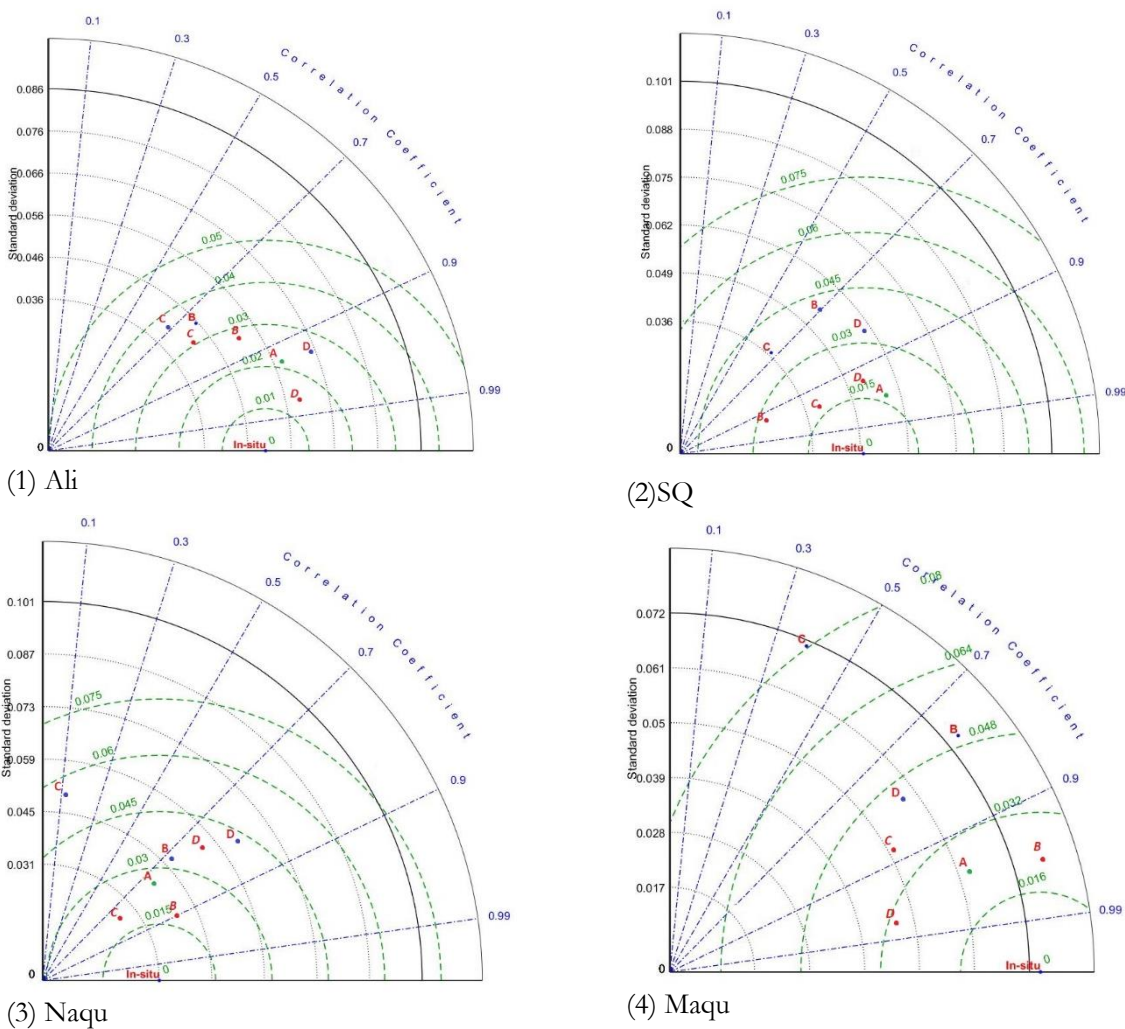


Figure 5.4: Taylor Diagrams: inter-comparison between profile soil moisture data and others.

Before in-situ climatology scaling, the other profile soil moisture showed a low correlation with in-situ data, although my product profile soil moisture, which scaled using CDF Matching based on in-situ climatology, estimated a little bit closer to the in-situ data, the root means squares and the standard deviation are always low. After climatology scaling, ERA-Interim data performed better, especially in Naqu and Maqu networks. The performance of SMAP becomes better, but it still worse than the others.

The discussion shows that the climatology scaling step is important, when it needs a reliable capture of in-situ data dynamics. Others, using CDF Matching to perform the depth scaling is simple and reliable.

## 6. CONCLUSION

In this study, a consistent surface and subsurface soil moisture product were produced by performing *satellites data merging*, *climatology scaling*, *objective blending* and *depth scaling*. As discussed in chapter 5, these procedures composed an integrated method to study surface and subsurface soil moisture using a sparse in-situ measurement network over Tibetan Plateau. First, different satellites observed data were merged into two satellites based products. Then the satellites products were constrained by in-situ climatology using CDF matching and the in-situ scaled land surface model simulated data. Next, all the input data were merged into a consistent surface soil moisture product. Last, the surface product was scaled using CDF matching to obtain a profile soil moisture form surface soil moisture product.

Beyond the typical data blending research; this research constrained the blending data sets with the in-situ climatology. It can eliminate the influence by using different land surface model simulation. It should be noticed that the choice of climate classification method can influence the in-situ climatology (Zeng et al., 2016). As discussed in chapter 5, the inter-comparison indicated that the scaling and blending strategy could constrain the overestimation of satellites data and keep the correlation with in-situ measured data. The consistent surface and subsurface soil moisture products presented a reliable data quality and captured the in-situ data dynamics. The climatology scaling ensured the variation of the final blended product. Also, the least squares method has unique advantages when compared with the simple averaged method over the arid areas. It shows better performance.

The depth scaling method predicted profile soil moisture from the blended consistent soil moisture product, can obtain a consistent profile soil moisture product keep the in-situ dynamics along with the surface product. It is a concise and efficient method to maximise the use of limited in-situ measured data. Others, the subsurface soil moisture states vary from station to station, for this reason, sometimes the zonal averaged profile soil cannot present a reliable estimation of profile soil moisture and the relationship between surface and subsurface.

## LIST OF REFERENCES

---

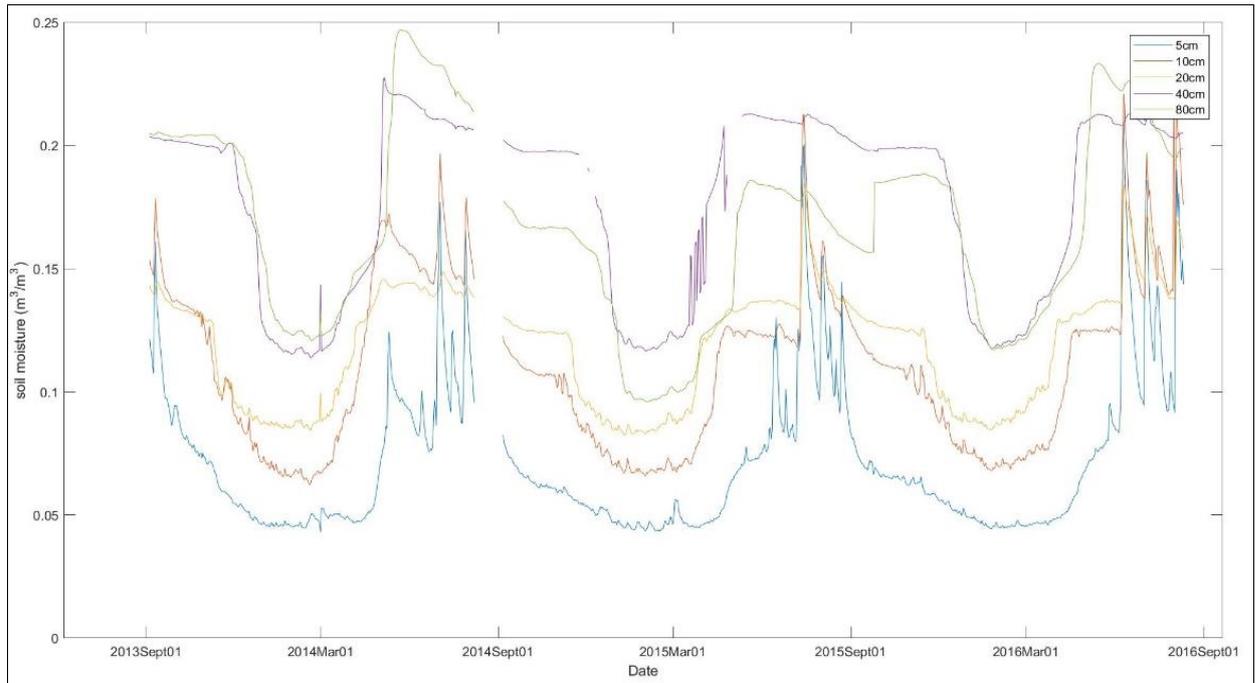
- Akbar, R., & Moghaddam, M. (2015). A combined active-passive soil moisture estimation algorithm with adaptive regularization in support of SMAP. *IEEE Transactions on Geoscience and Remote Sensing*, 53(6), 3312–3324. <https://doi.org/10.1109/TGRS.2014.2373972>
- Balsamo, G., Albergel, C., Beljaars, A., Boussetta, S., Brun, E., Cloke, H., ... Vitart, F. (2015). ERA-Interim/Land: A global land surface reanalysis data set. *Hydrology and Earth System Sciences*, 19(1), 389–407. <https://doi.org/10.5194/hess-19-389-2015>
- Bartalis, Z., Naeimi, V., & Wagner, W. (2008). ASCAT Soil Moisture Product Handbook. *Report Series, No. 15, Institute of Photogrammetry and Remote Sensing, Vienna University of Technology, Austria*, (15).
- Brocca, L., Hasenauer, S., Lacava, T., Melone, F., Moramarco, T., Wagner, W., ... Bittelli, M. (2011). Soil moisture estimation through ASCAT and AMSR-E sensors: An intercomparison and validation study across Europe. *Remote Sensing of Environment*, 115(12), 3390–3408. <https://doi.org/10.1016/j.rse.2011.08.003>
- Dee, D. P., Uppala, S. M., Simmons, A. J., Berrisford, P., Poli, P., Kobayashi, S., ... Vitart, F. (2011). The ERA-Interim reanalysis: Configuration and performance of the data assimilation system. *Quarterly Journal of the Royal Meteorological Society*, 137(656), 553–597. <https://doi.org/10.1002/qj.828>
- Dente, L., Ferrazzoli, P., Su, Z., van der Velde, R., & Guerriero, L. (2014). Combined use of active and passive microwave satellite data to constrain a discrete scattering model. *Remote Sensing of Environment*, 155, 222–238. <https://doi.org/10.1016/j.rse.2014.08.031>
- Dorigo, W. A., Gruber, A., De Jeu, R. A. M., Wagner, W., Stacke, T., Loew, A., ... Kidd, R. (2015). Evaluation of the ESA CCI soil moisture product using ground-based observations. *Remote Sensing of Environment*, 162, 380–395. <https://doi.org/10.1016/j.rse.2014.07.023>
- Dorigo, W. A., Scipal, K., Parinussa, R. M., Liu, Y. Y., Wagner, W., De Jeu, R. A. M., & Naeimi, V. (2010). Error characterisation of global active and passive microwave soil moisture datasets. *Hydrology and Earth System Sciences*, 14(12), 2605–2616. <https://doi.org/10.5194/hess-14-2605-2010>
- Drusch, M. (2007). Initializing numerical weather prediction models with satellite-derived surface soil moisture: Data assimilation experiments with ECMWF's integrated forecast system and the TMI soil moisture data set. *Journal of Geophysical Research Atmospheres*, 112(3), 1–14. <https://doi.org/10.1029/2006JD007478>
- Drusch, M., Wood, E. F., & Gao, H. (2005). Observation operators for the direct assimilation of TRMM microwave imager retrieved soil moisture. *Geophysical Research Letters*, 32(15), 32–35. <https://doi.org/10.1029/2005GL023623>
- Entekhabi, D., Njoku, E. G., O'Neill, P. E., Kellogg, K. H., Crow, W. T., Edelstein, W. N., ... Van Zyl, J. (2010). The Soil Moisture Active Passive (SMAP) Mission. *Proceedings of the IEEE*, 98(5), 704–716. <https://doi.org/10.1109/JPROC.2010.2043918>
- Gao, X., Wu, P., Zhao, X., Zhou, X., Zhang, B., Shi, Y., & Wang, J. (2013). Estimating soil moisture in gullies from adjacent upland measurements through different observation operators. *Journal of Hydrology*, 486, 420–429. <https://doi.org/10.1016/j.jhydrol.2013.02.007>
- Gao, X., Zhao, X., Brocca, L., Lv, T., Huo, G., & Wu, P. (2016). Depth scaling of soil moisture content from surface to profile: multi-station testing of observation operators. *Hydrology and Earth System Sciences Discussions*, (November), 1–28. <https://doi.org/10.5194/hess-2016-617>
- Han, E., Heathman, G. C., Merwade, V., & Cosh, M. H. (2012). Application of observation operators for field scale soil moisture averages and variances in agricultural landscapes. *Journal of Hydrology*, 444–445, 34–50. <https://doi.org/10.1016/j.jhydrol.2012.03.035>
- Han, E., Merwade, V., & Heathman, G. C. (2012). Application of data assimilation with the Root Zone Water Quality Model for soil moisture profile estimation in the upper Cedar Creek, Indiana. *Hydrological Processes*, 26(11), 1707–1719. <https://doi.org/10.1002/hyp.8292>
- Hengl, T., De Jesus, J. M., MacMillan, R. A., Batjes, N. H., Heuvelink, G. B. M., Ribeiro, E., ... Gonzalez, M. R. (2014). SoilGrids1km - Global soil information based on automated mapping. *PLoS ONE*, 9(8). <https://doi.org/10.1371/journal.pone.0105992>
- Hengl, T., Mendes de Jesus, J., Heuvelink, G. B. M., Ruiperez Gonzalez, M., Kilibarda, M., Blagotić, A., ... Kempen, B. (2017). SoilGrids250m: Global gridded soil information based on machine learning. *Plos One*, 12(2), e0169748. <https://doi.org/10.1371/journal.pone.0169748>
- Holmes, T. R. H., De Jeu, R. A. M., Owe, M., & Dolman, A. J. (2009). Land surface temperature from Ka band (37 GHz) passive microwave observations. *Journal of Geophysical Research Atmospheres*, 114(4), 1–

15. <https://doi.org/10.1029/2008JD010257>
- Imaoka, K., Kachi, M., Fujii, H., Murakami, H., Hori, M., Ono, A., ... Shimoda, H. (2010). Global change observation mission (GCOM) for monitoring carbon, water cycles, and climate change. *Proceedings of the IEEE*, 98(5), 717–734. <https://doi.org/10.1109/JPROC.2009.2036869>
- Imaoka, K., Maeda, T., Kachi, M., Kasahara, M., Ito, N., Nakagawa, K., ... X, X. (2012). Status of AMSR2 instrument on GCOM-W1. *Earth Observing Missions and Sensors: Development, Implementation, and Characterization II*, 8528(March), 1–6. <https://doi.org/10.1117/12.977774>
- Kalman, R. E. (1960). A New Approach to Linear Filtering and Prediction Problems. *Journal of Basic Engineering*, 82(1), 35. <https://doi.org/10.1115/1.3662552>
- Kang, S., Xu, Y., You, Q., Flügel, W.-A., Pepin, N., & Yao, T. (2010). Review of climate and cryospheric change in the Tibetan Plateau. *Environmental Research Letters*, 5(1), 15101. <https://doi.org/10.1088/1748-9326/5/1/015101>
- Kerr, Y. H., Waldteufel, P., Richaume, P., Wigneron, J. P., Ferrazzoli, P., Mahmoodi, A., ... Delwart, S. (2012). The SMOS Soil Moisture Retrieval Algorithm. *Geoscience and Remote Sensing*, 50(5), 1384–1403. <https://doi.org/10.1109/TGRS.2012.2184548>
- Kerr, Y. H., Waldteufel, P., Wigneron, J. P., Delwart, S., Cabot, F., Boutin, J., ... Mecklenburg, S. (2010). The SMOS Mission: New Tool for Monitoring Key Elements of the Global Water Cycle. *Proceedings of the IEEE*, 98(5), 666–687. <https://doi.org/10.1109/jproc.2010.2043032>
- Kerr, Y. H., Waldteufel, P., Wigneron, J. P., Martinuzzi, J. M., Font, J., & Berger, M. (2001). Soil moisture retrieval from space: The Soil Moisture and Ocean Salinity (SMOS) mission. *IEEE Transactions on Geoscience and Remote Sensing*, 39(8), 1729–1735. <https://doi.org/10.1109/36.942551>
- Liu, Y. Y., Dorigo, W. A., Parinussa, R. M., De Jeu, R. A. M., Wagner, W., McCabe, M. F., ... Van Dijk, A. I. J. M. (2012). Trend-preserving blending of passive and active microwave soil moisture retrievals. <https://doi.org/10.1016/j.rse.2012.03.014>
- Liu, Y. Y., Parinussa, R. M., Dorigo, W. A., De Jeu, R. A. M., Wagner, W., M. Van Dijk, A. I. J., ... Evans, J. P. (2011). Developing an improved soil moisture dataset by blending passive and active microwave satellite-based retrievals. *Hydrology and Earth System Sciences*, 15(2), 425–436. <https://doi.org/10.5194/hess-15-425-2011>
- Ma, Y., Kang, S., Zhu, L., Xu, B., Tian, L., & Yao, T. (2008). Roof of the World: Tibetan observation and research platform. *Bulletin of the American Meteorological Society*, 89(10), 1487–1492. <https://doi.org/10.1175/2008BAMS2545.1>
- Ma, Y., Ma, W., Zhong, L., Hu, Z., Li, M., & Zhu, Z. (2017). Monitoring and Modeling the Tibetan Plateau 's climate system and its impact on East Asia. *Nature Publishing Group*, 1–6. <https://doi.org/10.1038/srep44574>
- Meesters, A. G. C. A., De Jeu, R. A. M., & Owe, M. (2005). Analytical derivation of the vegetation optical depth from the microwave polarization difference index. *IEEE Geoscience and Remote Sensing Letters*, 2(2), 121–123. <https://doi.org/10.1109/LGRS.2005.843983>
- Milly, P. C. D., & Dunne, K. A. (1994). Sensitivity of the global water cycle to the water-holding capacity of land. *Journal of Climate*. [https://doi.org/10.1175/1520-0442\(1994\)007<0506:SOTGWC>2.0.CO;2](https://doi.org/10.1175/1520-0442(1994)007<0506:SOTGWC>2.0.CO;2)
- Mo, T., Choudhury, B. J., Schmugge, T. J., Wang, J. R., & Jackson, T. J. (1982). A model for microwave emission from vegetation-covered fields. *Journal of Geophysical Research*, 87(1), 11229–11237. <https://doi.org/10.1029/JC087iC13p11229>
- Naeimi, V., Scipal, K., Bartalis, Z., Hasenauer, S., & Wagner, W. (2009). An improved soil moisture retrieval algorithm for ERS and METOP scatterometer observations. *IEEE Transactions on Geoscience and Remote Sensing*, 47(7), 1999–2013. <https://doi.org/10.1109/TGRS.2008.2011617>
- Njoku, E. G., Ashcroft, P., Chan, T. K., & Li, L. (2005). Global survey and statistics of radio-frequency interference in AMSR-E land observations. *IEEE Transactions on Geoscience and Remote Sensing*, 43(5), 938–946. <https://doi.org/10.1109/TGRS.2004.837507>
- Njoku, E. G., Jackson, T. J., Lakshmi, V., Chan, T. K., & Nghiem, S. V. (2003). Soil moisture retrieval from AMSR-E. *IEEE Transactions on Geoscience and Remote Sensing*, 41(2 PART 1), 215–228. <https://doi.org/10.1109/TGRS.2002.808243>
- O'Neill, P., Chan, S., Njoku, E., Jackson, T., & Bindlish, R. (2014). Soil Moisture Active Passive (SMAP) Algorithm Theoretical Basis Document Level 2 & 3 Soil Moisture (Passive) Data Products. Retrieved August 14, 2017, from <http://smap.jpl.nasa.gov/documents/>
- Owe, M., de Jeu, R., & Holmes, T. (2008). Multisensor historical climatology of satellite-derived global land surface moisture. *Journal of Geophysical Research: Earth Surface*, 113(1), 1–17. <https://doi.org/10.1029/2007JF000769>

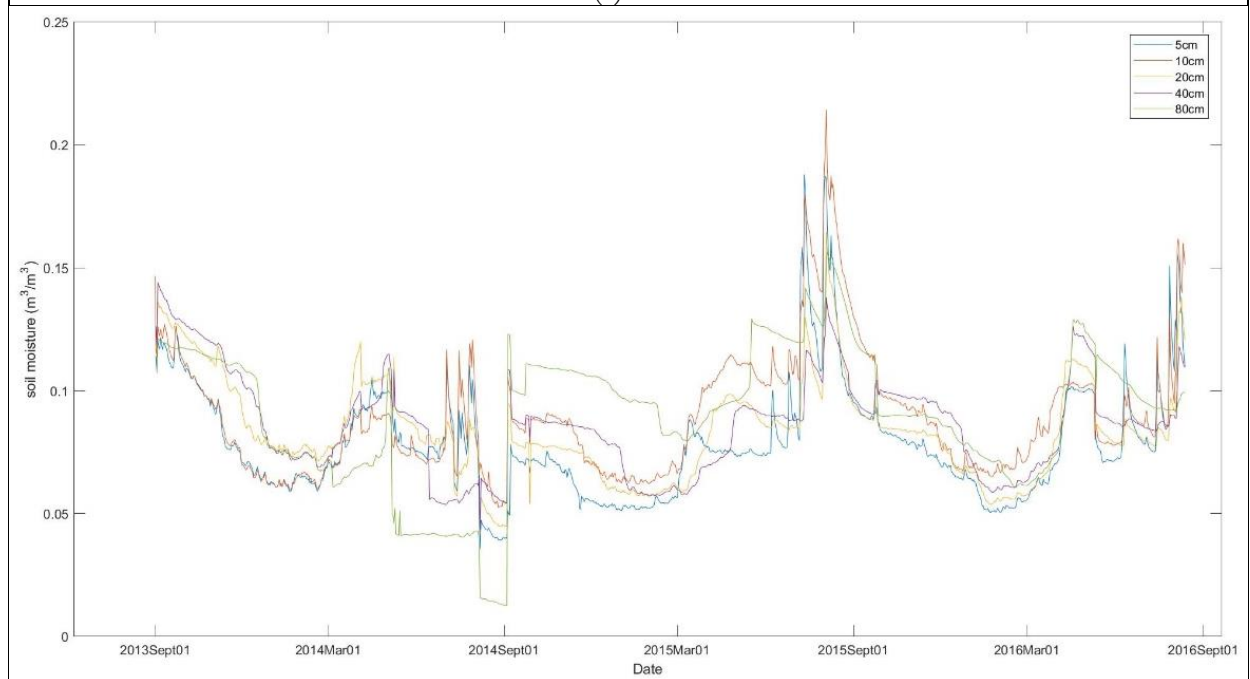
- Panciera, R., Walker, J. P., Jackson, T. J., Gray, D. A., Tanase, M. A., Ryu, D., ... Hacker, J. M. (2014). The Soil Moisture Active Passive Experiments ( SMAPEX ): Toward Soil Moisture Retrieval From the SMAP Mission, *52*(1), 490–507.
- Petropoulos, G. (2013). *Remote Sensing of Energy Fluxes and Soil Moisture Content* (1st ed.). Baton Rouge: CRC Press. <https://doi.org/10.1201/b15610>
- Polcher, J. (1995). Sensitivity of Tropical Convection to Land Surface Processes. *Journal of the Atmospheric Sciences*. [https://doi.org/10.1175/1520-0469\(1995\)052<3143:SOTCTL>2.0.CO;2](https://doi.org/10.1175/1520-0469(1995)052<3143:SOTCTL>2.0.CO;2)
- Reichle, R. H., & Koster, R. D. (2004). Bias reduction in short records of satellite soil moisture. *Geophysical Research Letters*, *31*(19), 2–5. <https://doi.org/10.1029/2004GL020938>
- Reynolds, C. A., Jackson, T. J., & Rawls, W. J. (2000). Estimating soil water-holding capacities by linking the Food and Agriculture Organization soil map of the world with global pedon databases and continuous pedotransfer functions. *Water Resources Research*, *36*(12), 3653–3662. <https://doi.org/10.1029/2000WR900130>
- Rodell, M., Houser, P. R., Jambor, U., Gottschalck, J., Mitchell, K., Meng, C.-J., ... Toll, D. (2004). The Global Land Data Assimilation System. *Bulletin of the American Meteorological Society*, *85*(3), 381–394. <https://doi.org/10.1175/BAMS-85-3-381>
- Sorenson, H. W. (1970). Least-squares estimation: from Gauss to Kalman. *IEEE Spectrum*, *7*(7), 63–68. <https://doi.org/10.1109/MSPEC.1970.5213471>
- Stoffelen, A. (1998). Toward the true near-surface wind speed: Error modeling and calibration using triple collocation. *Journal of Geophysical Research*, *103*(15), 7755–7766. <https://doi.org/10.1029/97JC03180>
- Su, Z., De Rosnay, P., Wen, J., Wang, L., & Zeng, Y. (2013). Evaluation of ECMWF's soil moisture analyses using observations on the Tibetan Plateau. *Journal of Geophysical Research Atmospheres*, *118*(11), 5304–5318. <https://doi.org/10.1002/jgrd.50468>
- Su, Z., Troch, P. A., & DeTroch, F. P. (1997). Remote sensing of bare surface soil moisture using EMAC/ESAR data. *International Journal of Remote Sensing*, *18*(10), 2105–2124. <https://doi.org/10.1080/014311697217783>
- Su, Z., Wen, J., Dente, L., Van Der Velde, R., Wang, L., Ma, Y., ... Hu, Z. (2011). The tibetan plateau observatory of plateau scale soil moisture and soil temperature (Tibet-Obs) for quantifying uncertainties in coarse resolution satellite and model products. *Hydrology and Earth System Sciences*, *15*(7), 2303–2316. <https://doi.org/10.5194/hess-15-2303-2011>
- Talagrand, O. (1997). Assimilation of Observations, an Introduction. *Journal of the Meteorological Society of Japan*, *75*(1B), 191–209. Retrieved from [https://www.jstage.jst.go.jp/article/jmsj1965/75/1B/75\\_1B\\_191/\\_pdf](https://www.jstage.jst.go.jp/article/jmsj1965/75/1B/75_1B_191/_pdf)
- Wagner, W., Dorigo, W., de Jeu, R., Fernandez, D., Benveniste, J., Haas, E., & Ertl, M. (2012). Fusion of Active and Passive Microwave Observations To Create an Essential Climate Variable Data Record on Soil Moisture. *ISPRS Annals of Photogrammetry, Remote Sensing and Spatial Information Sciences*. <https://doi.org/10.5194/isprsannals-I-7-315-2012>
- Wagner, W., Hahn, S., Kidd, R., Melzer, T., Bartalis, Z., Hasenauer, S., ... Rubel, F. (2013). The ASCAT soil moisture product: A review of its specifications, validation results, and emerging applications. *Meteorologische Zeitschrift*, *22*(1), 5–33. <https://doi.org/10.1127/0941-2948/2013/0399>
- Wang, J. R., & Schmugge, T. J. (1980). An empirical model for the complex dielectric permittivity of soils as a function of water content. *IEEE Transactions on Geoscience and Remote Sensing*, *GE-18*(4), 288–295. <https://doi.org/10.1109/TGRS.1980.350304>
- Wen, J., & Su, Z. (2003). The estimation of soil moisture from ERS wind scatterometer data over the Tibetan plateau. *Physics and Chemistry of the Earth*, *28*(1–3), 53–61. [https://doi.org/10.1016/S1474-7065\(03\)00007-X](https://doi.org/10.1016/S1474-7065(03)00007-X)
- Wigneron, J. P., Kerr, Y., Waldteufel, P., Saleh, K., Escorihuela, M. J., Richaume, P., ... Schwank, M. (2007). L-band Microwave Emission of the Biosphere (L-MEB) Model: Description and calibration against experimental data sets over crop fields. *Remote Sensing of Environment*, *107*(4), 639–655. <https://doi.org/10.1016/j.rse.2006.10.014>
- Yang, K., Qin, J., Zhao, L., Chen, Y., Tang, W., Han, M., ... Lin, C. (2013). A multiscale soil moisture and freeze-thaw monitoring network on the third pole. *Bulletin of the American Meteorological Society*, *94*(12), 1907–1916. <https://doi.org/10.1175/BAMS-d-12-00203.1>
- Yang, K., Wu, H., Qin, J., Lin, C., Tang, W., & Chen, Y. (2014). Recent climate changes over the Tibetan Plateau and their impacts on energy and water cycle: A review. *Global and Planetary Change*, *112*, 79–91. <https://doi.org/10.1016/j.gloplacha.2013.12.001>
- Yilmaz, M. T., Crow, W. T., Anderson, M. C., & Hain, C. (2012). An objective methodology for merging

- satellite- and model-based soil moisture products. *Water Resources Research*, 48(11), 1–15.  
<https://doi.org/10.1029/2011WR011682>
- Zeng, J., Li, Z., Chen, Q., & Bi, H. (2014). A simplified physically-based algorithm for surface soil moisture retrieval using AMSR-E data. *Frontiers of Earth Science*, 8(3), 427–438.  
<https://doi.org/10.1007/s11707-014-0412-4>
- Zeng, J., Li, Z., Chen, Q., Bi, H., Qiu, J., & Zou, P. (2015). Evaluation of remotely sensed and reanalysis soil moisture products over the Tibetan Plateau using in-situ observations. *Remote Sensing of Environment*, 163, 91–110. <https://doi.org/10.1016/j.rse.2015.03.008>
- Zeng, Y., Su, Z., Van Der Velde, R., Wang, L., Xu, K., Wang, X., & Wen, J. (2016). Blending satellite observed, model simulated, and in situ measured soil moisture over Tibetan Plateau. *Remote Sensing*, 8(3), 1–22. <https://doi.org/10.3390/rs8030268>
- Zhan, X., Liu, J., & Zhao, L. (2016). *Soil Moisture Operational Product System (SMOPS) Algorithm Theoretical Basis Document*.
- Zhao, H., Zeng, Y., Lv, S., & Su, Z. (2018). Analysis of Soil Hydraulic and Thermal Properties for Land Surface Modelling over the Tibetan Plateau, (January), 1–40.
- Zwieback, S., Scipal, K., Dorigo, W., & Wagner, W. (2012). Structural and statistical properties of the collocation technique for error characterization. *Nonlinear Processes in Geophysics*, 19(1), 69–80.  
<https://doi.org/10.5194/npg-19-69-2012>

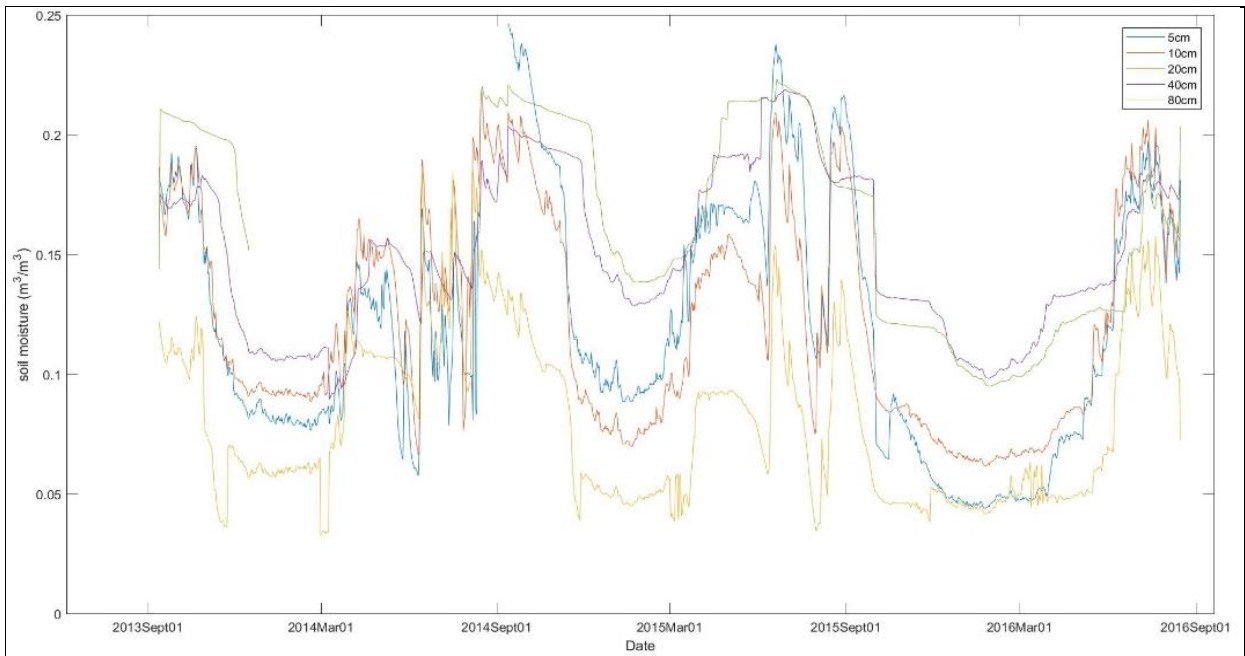
# APPENDIX 1



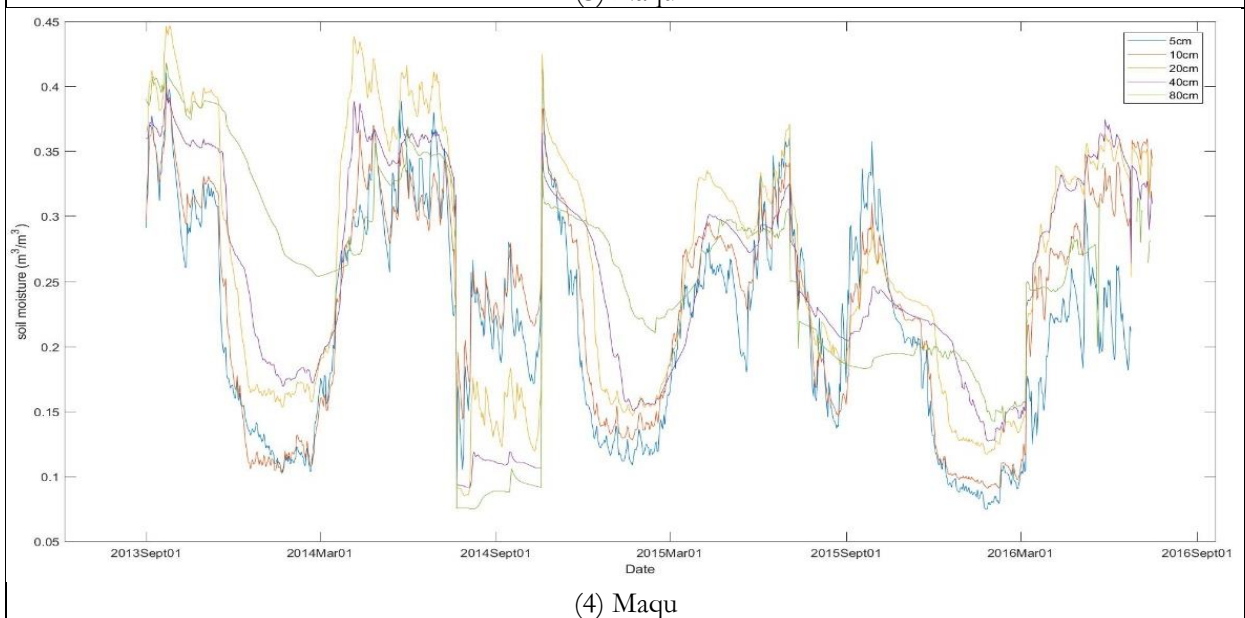
(1) Ali



(2) SQ



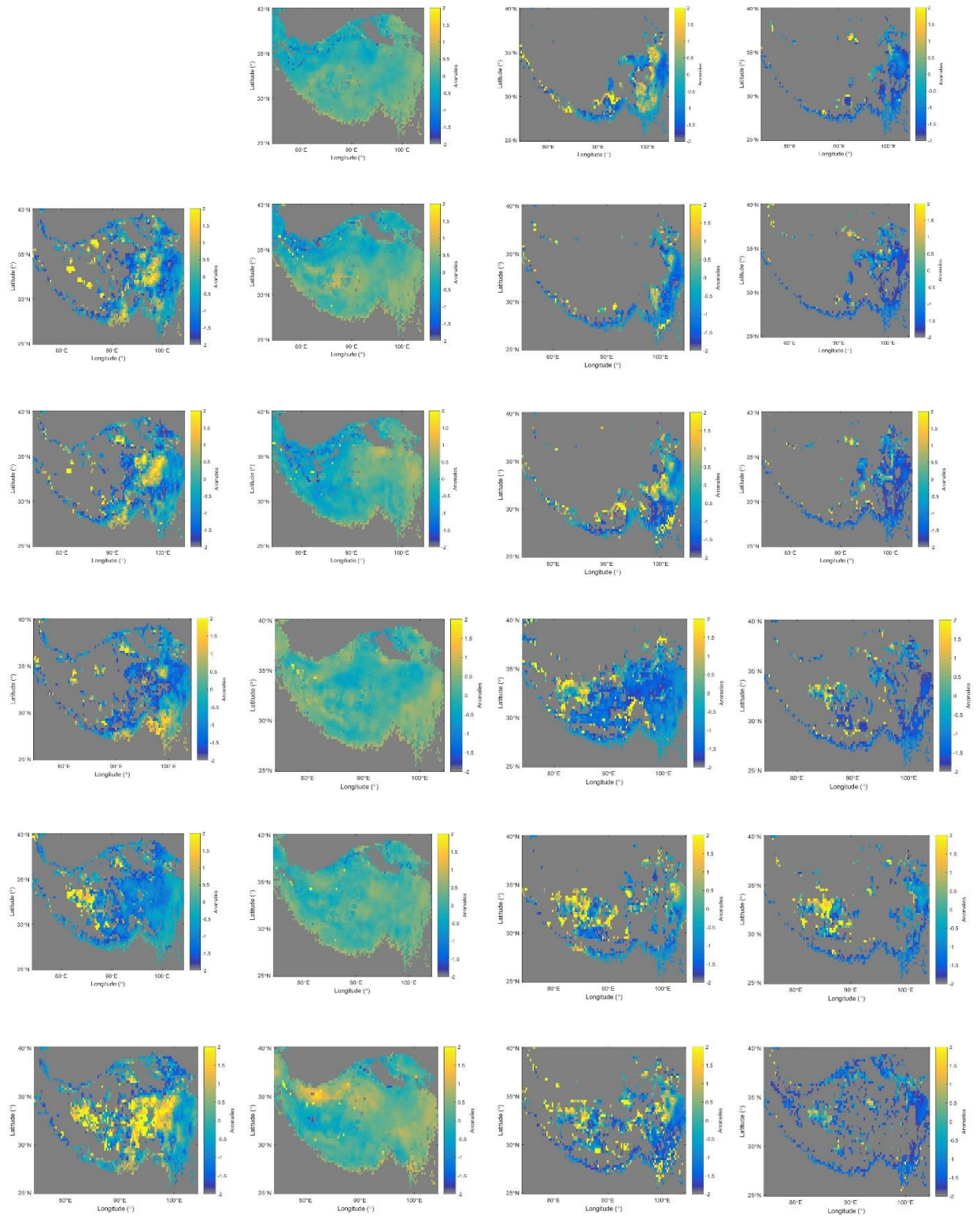
(3) Naqu

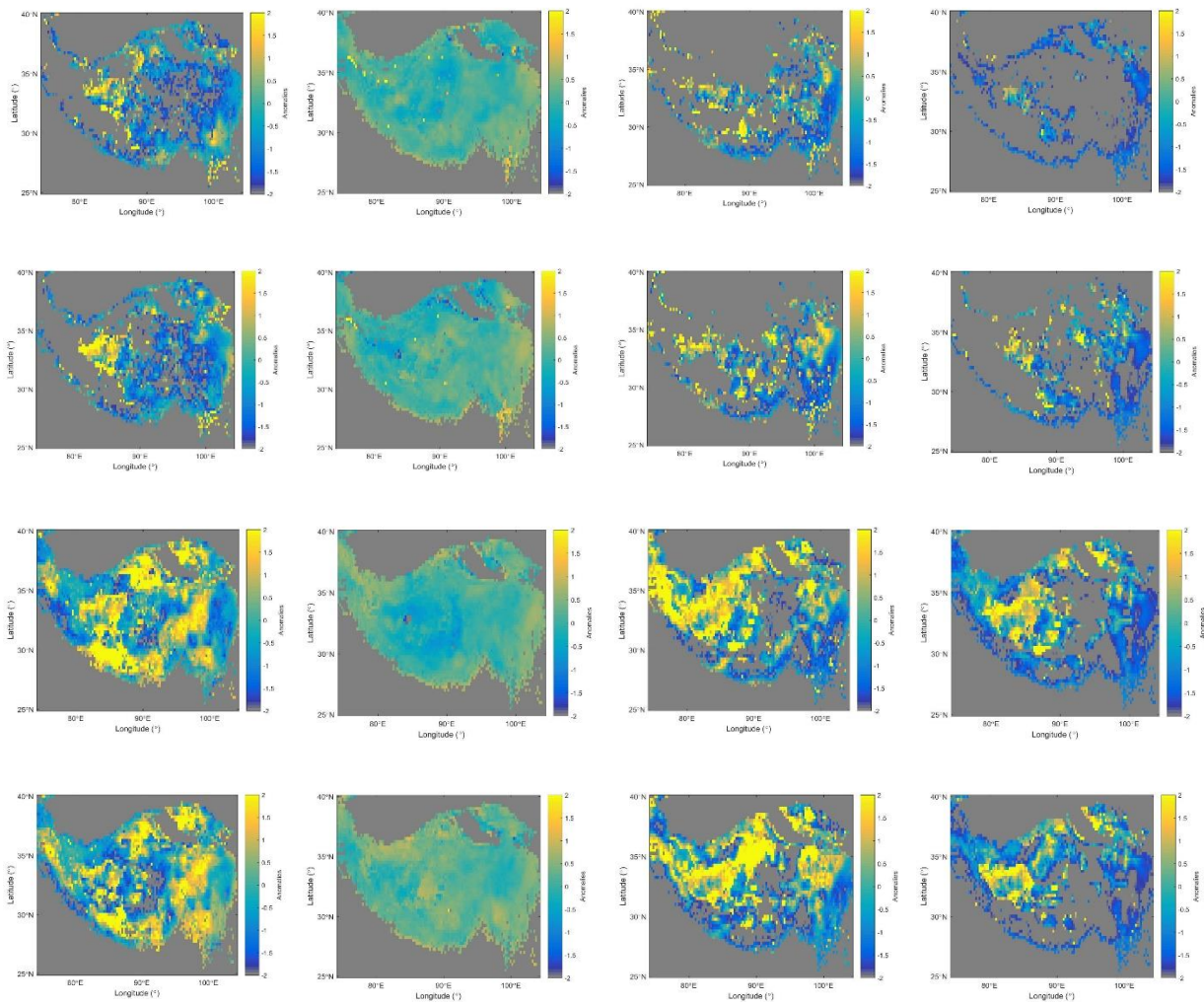


(4) Maqu

Appendix Figure 1: Time Series of In-situ Measured Surface and Sub surface Soil Moisture

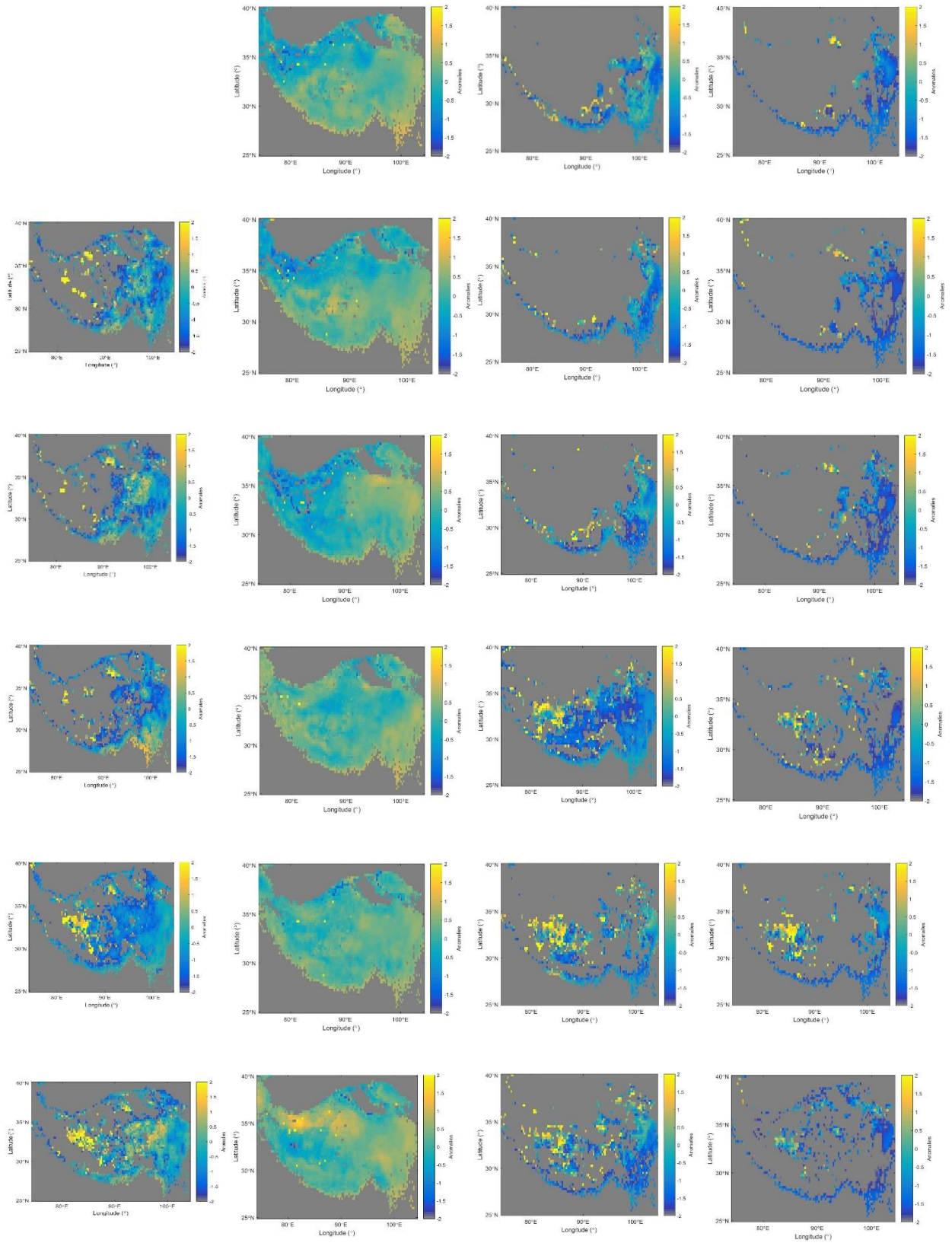
# APPENDIX 2

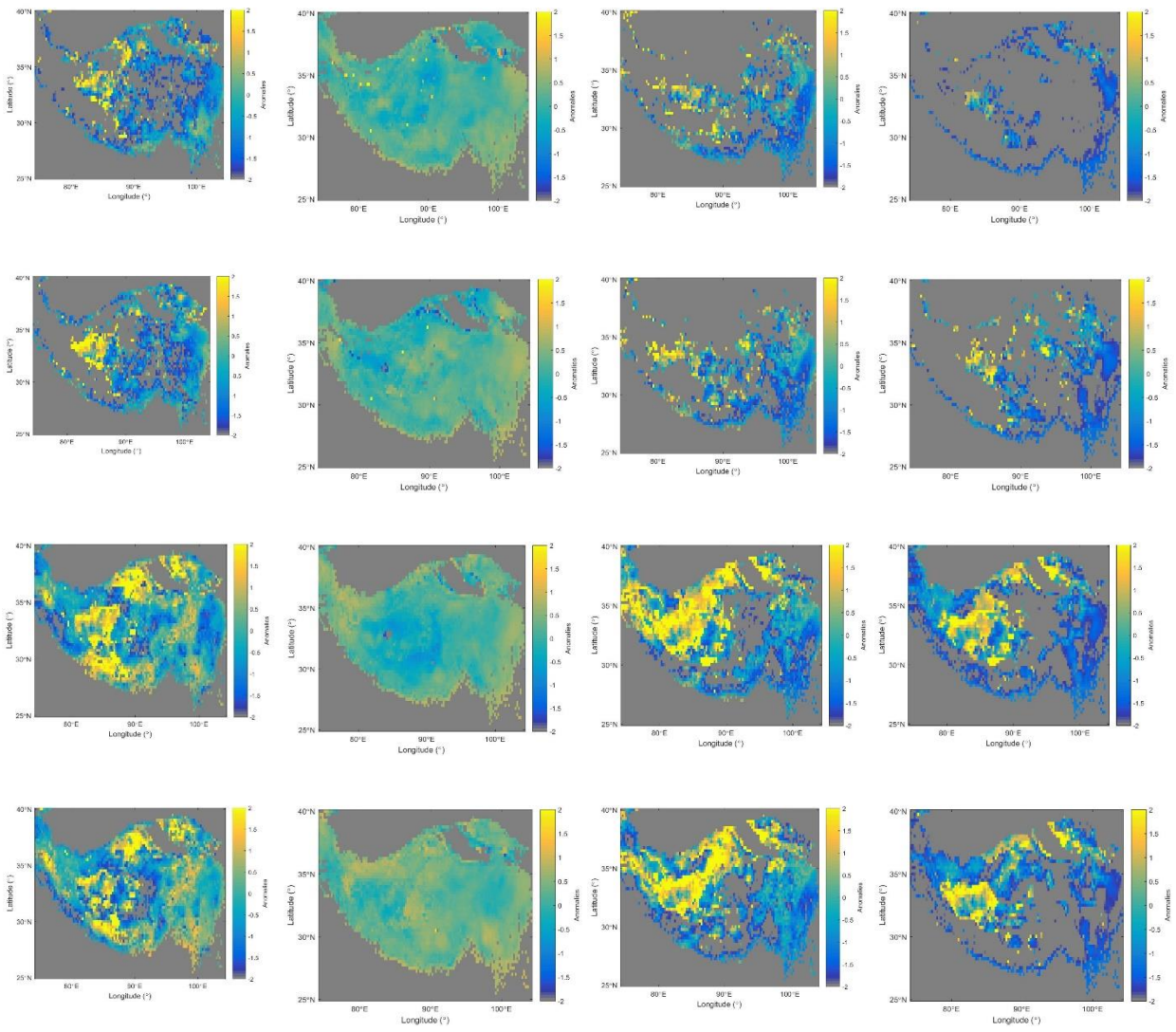




Appendix Figure 2 Anomalies of Blended Surface Soil Moisture

# APPENDIX 3





Appendix Figure 3 Anomalies of Profile Soil Moisture